JGR Solid Earth

RESEARCH ARTICLE
10.1029/2019JB017394

Key Points:
- Fracturing related to local extension by fault interaction in a convergent regional setting controls fluid flow in a geothermal system
- Numerical simulations corroborate the impact of structural process driving a local increase in convection and the rising of thermal waters
- Convection enhanced by fracturing can result in temperature values profitable for energy production in low-temperature geothermal resources

Supporting Information:
- Supporting Information S1

Correspondence to:
P. Fabbri,
paolo.fabbri@unipd.it

Citation:
Pola, M., Cacace, M., Fabbri, P., Piccinini, L., Zampieri, D., & Torresan, F. (2020). Fault control on a thermal anomaly: Conceptual and numerical modeling of a low-temperature geothermal system in the Southern Alps foreland basin (NE Italy). *Journal of Geophysical Research: Solid Earth*, *125*, e2019JB017394. https://doi.org/10.1029/2019JB017394

Received 18 JAN 2019
Accepted 16 APR 2020
Accepted article online 20 APR 2020

Fault Control on a Thermal Anomaly: Conceptual and Numerical Modeling of a Low-Temperature Geothermal System in the Southern Alps Foreland Basin (NE Italy)

Marco Pola[1], Mauro Cacace[2], Paolo Fabbri[3,4], Leonardo Piccinini[3,4], Dario Zampieri[3,4], and Filippo Torresan[3]

[1]Croatian Geological Survey, Zagreb, Croatia, [2]Helmholtz Centre Potsdam, GFZ German Research Centre for Geosciences, Telegrafenberg, Potsdam, Germany, [3]Department of Geosciences, Università degli Studi di Padova, Padova, Italy, [4]Geothermal System Hydrostructures (GSH), Interdepartmental Centre "Giorgio Levi Cases" for Energy Economics and Technology, Università degli Studi di Padova, Padova, Italy

Abstract The interest on low-temperature geothermal resources is progressively increasing since their renewability and widespread availability. Despite their frequency, these resources and their development have been only partially investigated. This paper unravels the major physical processes driving a low-temperature geothermal resource in NE Italy (Euganean Geothermal System) through conceptual and numerical modeling. Dense fracturing associated to regional fault zones and a relay ramp enhances regional to local flow of thermal waters. Their rapid upwelling in the Euganean Geothermal Field is favored by open extensional fractures deforming the relay ramp. The water (65–86 °C) is intensively exploited for balneotherapy, rendering it a profitable resource. Three-dimensional coupled flow and heat transport numerical simulations based on this conceptual model are performed. Despite the presence of a uniform basal heat flow, a thermal anomaly corresponding to field observations develops in the modeling domain reproducing the relay ramp. Intensive fracturing extending across a wide area and a slightly anomalous heat flow favors a local increase in convection that drives the upwelling of deep-seated hot waters.
The simulations corroborate and refine the conceptual model, revealing that water of up to 115 °C is likely to be found in the unexplored part of the thermal field. This study furthers knowledge on fault-controlled low-temperature geothermal resources where the geological setting could enhance local convection without anomalous heat flows, creating temperatures favorable for energy production. Conceptual and numerical modeling based on solid geological and hydrogeological reconstructions can offer a support tool for further detailed explorations of these prominent resources.

1. Introduction

The most important and profitable geological resources are associated with the circulation and storage of deep-seated fluids (i.e., ore deposits of hydrothermal minerals, petroleum resources, and geothermal resources). These result from several concurring processes related to regional and local geological settings and to physical and chemical features of fluids. Geothermal resources are used for energy production, heating, and industrial applications (Lund & Boyd, 2016). A detailed exploration is crucial to understanding the interaction of physical, chemical, and geological processes in the associated geothermal system and to planning a sustainable utilization of the resource. The interplay of these processes can be evaluated using numerical models that integrate 3-D reconstructions of the geological settings into the first-order physical principles of coupled fluid and heat transport (e.g., Baiocchi et al., 2013; Brehme et al., 2016; Magri et al., 2012; Scheck-Wenderoth et al., 2014). High-temperature geothermal resources have historically been the most explored and modeled due to their great economic utility and long-term exploitation (e.g., Della Vedova et al., 2008; Ingebritsen et al., 2010; Scott et al., 2016). Although they are widespread worldwide, low-temperature geothermal resources have been less investigated thus far (e.g., Baietto et al., 2008; Montanari et al., 2017; Volpi et al., 2017). Despite the usual classifications based on temperature (Dickson & Fanelli, 2013), geothermal resources can be cataloged by their geological characteristics (i.e., geological settings, heat and fluid sources, and migration pathways), referred to as geothermal play. Two groups

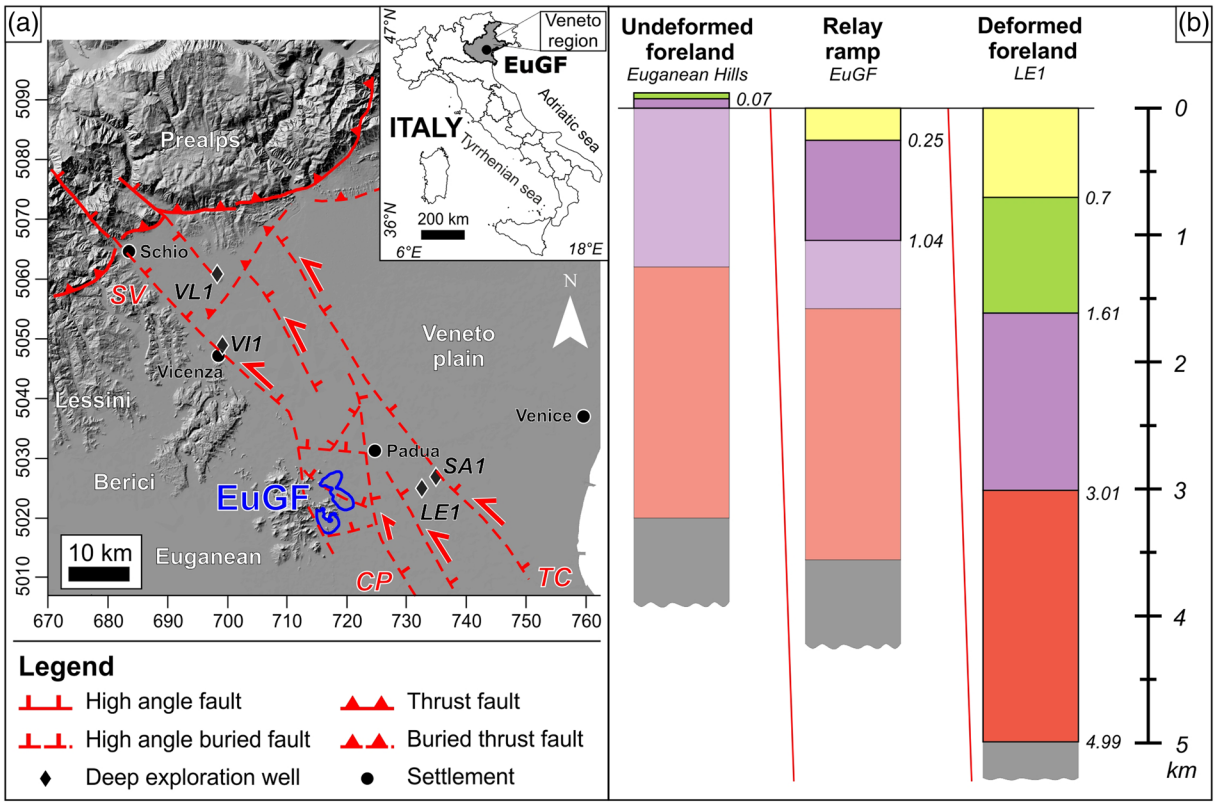

Figure 1. Geological setting of the central Veneto region (NE Italy). The structural sketch (a; coordinates in UTM zone 32 N system using the WGS84 datum) shows the main segments of the Schio-Vicenza fault system (SV: Schio-Vicenza fault; CP: Conselve-Pomposa fault; TC: Travettore-Codevigo fault) and their interaction zone, where the Euganean Geothermal Field (EuGF) is located. The hydrocarbon exploration wells (black diamonds; VL1: Villaverla 1; VI1: Vicenza 1; LE1: Legnaro 1; SA1: Sant'Angelo Piove di Sacco 1) and the main cities of the investigated area (black circles) are reported. The hydrostratigraphic sketch (b) shows the eastward deepening of the units accommodated by the fault system. The depths are reconstructed from stratigraphic logs (LE1, EuGF) or geological maps (Euganean Hills). For the legend of the units the reader is referred to Figure 2. The inferred data are shown in lighter colors.

based on the main physical process producing the play type are established (Moeck, 2014). Conduction-dominated geothermal plays occur in tectonically inactive areas (i.e., passive continental margins, intracratonic basins, and foreland basins), while convection-dominated geothermal plays are associated with active volcanism and/or tectonism. For the latter type of resources, most of the fluid originates from the infiltration of meteoric water, heat flows are strong, and active faults and their subsidiary fracture networks are the preferential paths for fluid circulation. Fracturing varies the permeability field of reservoir, which can be locally enhanced by orders of magnitude from the original undeformed protolith (e.g., Bense et al., 2013; Faulkner et al., 2010). The resulting geological and hydrogeological heterogeneities and convection add to the complexity of the system, demanding detailed conceptual and numerical models.

The Euganean Geothermal System (EuGS) is one of the most important water-dominated low-temperature geothermal systems in Europe. It extends through the central part of the Veneto region (Italy), and its main outflow area is the Euganean Geothermal Field (EuGF). The thermal field covers a plain band of 25 km^2 located southwest of the city of Padua (Figure 1a). Its thermal waters have naturally flowed into springs at least since 34 ka (Pola et al., 2011), having been used for therapeutic purposes since Roman times (Bassani et al., 2012). Their forced exploitation by wells started at the end of the nineteenth century. The increased anthropic pressure into the twentieth century caused a sharp decline in potentiometric levels drying all springs (Fabbri et al., 2017; Pola et al., 2015). Approximately 600 wells have been drilled in the EuGF since the 1900s, and 150 wells were active in 2017, exploiting 14.9×10^6 m^3. The water is mainly used for balneotherapy in 95 spa facilities, constituting the largest spa center in Europe. Several hundreds of thousand tourists attend the facilities, generating an income of 300 million € per year (Consorzio Terme

Euganee, 2016). Heating for resorts, floriculture, and aquaculture represents secondary uses. Because of the natural, social, and economic relevance of this thermal resource, several studies have been carried out since the eighteenth century (Mandruzzato, 1789). Prior studies have investigated the geochemical features of the thermal waters (Gherardi et al., 2000; Mayer et al., 2015; Norton & Panichi, 1978) and the geological, hydrogeological, and thermal settings of the EuGF (Antonelli et al., 1993; Fabbri, 1997, 2001; Fabbri & Trevisani, 2005; Pola et al., 2016). Conversely, a proper regional geological and hydrogeological reconstruction of the Veneto subsurface is lacking. Hydrocarbon exploration wells are few (Figure 1a) and have been investigated with stratigraphic and thermal logs while geophysical data (i.e., seismic sections and gravimetric maps) are relatively sparse. A first attempt to develop a multiscale conceptual model of the EuGS was recently advanced by Pola et al. (2015). This work benefits from and revises the available model by relating (i) regional and local geological settings, (ii) geochemical and isotopic features of the water, (iii) regional and local hydrogeological settings including hydraulic properties of the bedrock, and (iv) physical principles of hydrothermal dynamics that are likely to occur in the system. The updated conceptual model will be presented in the first section of this study. Subsequently, its reliability in explaining the first-order characteristics of hydrothermal system dynamics will be tested by means of 3-D regional coupled fluid flow and heat transport numerical simulations. The results will enable a first quantification, both in terms of magnitudes and interconnections, of major processes driving the Euganean thermal resource. These results will prove beneficial in improving current knowledge on low-temperature geothermal systems in fractured carbonate rocks.

1.1. Regional Geological Setting

The stratigraphic sequence of central Veneto (Antonelli et al., 1990) can be simplified as follows: (i) pre-Permian low-grade metamorphic basement made of phyllites, (ii) Permian to Middle Triassic clastic and evaporitic rocks and secondary carbonate rocks, (iii) Late Triassic to Early Cretaceous dolostones and limestones, (iv) Early Cretaceous to Eocene mudstones and limestones locally interlayered with or intruded by Paleogene volcanic bodies, (v) Oligocene to Miocene clastic rocks and secondary limestones and mudstones, and (vi) Quaternary usually alluvial sediments. The stratigraphic setting of the EuGF was established up to 1 km deep through the stratigraphic logs of the thermal wells (Antonelli et al., 1993; Fabbri et al., 2017). It matches the described regional sequence: the Quaternary alluvial cover is up to 200 m thick, and explored rocky formations are composed of Late Triassic to Early Oligocene sedimentary rocks locally intruded by Late Eocene to Early Oligocene trachyte and rhyolite (secondarily, basalt and latite) cropping out into the Euganean Hills (Bartoli et al., 2015; Cucato et al., 2012). The sedimentary formations are Late Cretaceous-Early Oligocene marly limestones and mudstones, Late Jurassic-Early Cretaceous limestones, and Late Triassic-Middle Jurassic limestones and dolostones. Beneath these formations, Permian-Triassic units, which bear a few evaporite levels with predominantly gypsum or anhydrite, and the pre-Permian basement are likely to occur since they were explored in a nearby, 5 km deep, hydrocarbon exploration well (LE 1 in Figure 1).

The regional structural setting can be subdivided into three main structural domains bordered by regional faults (Figure 1a; e.g., Massironi et al., 2006; Viganò et al., 2008; Zampieri, 1995). The Veneto Eastern Southern Alps (Prealps) are divided from their foreland by ENE-WSW trending, NNW dipping thrusts. The NW-SE to NNW-SSE trending, NE dipping, high-angle Schio-Vicenza fault system (SVFS; Pola et al., 2014) separates the undeformed foreland from its deformed sector (Lessini-Berici-Euganean and Veneto plain blocks, respectively). The SVFS accommodated the multiphase deformation of the foreland since the Mesozoic (Fantoni et al., 2002; Fantoni & Franciosi, 2010). The result was an eastward subsiding mosaic of blocks (Figure 1b) affected by a differential southward bending increasing from minor in the study area to prominent toward their southern sectors (i.e., southern Veneto region; Pola, Ricciato, et al., 2014).

To the south of Padua, in correspondence with the EuGF (Figure 1a), a relay ramp develops between two Jurassic-Paleogene normal fault segments reactivated as strike-slip faults from the Neogene to the Present. The relay ramp deformed once again as an area of localized extension, enhancing its fracturing. Favorable conditions for the rise of deep-seated fluids generally occur in relay ramps or interaction zones as established in global geothermal and oil fields (e.g., Faulds et al., 2013; Fossen & Rotevatn, 2016; Rotevatn & Peacock, 2018; Rowland & Sibson, 2004). The local extension of the SVFS relay ramp develops a Hill-type mixed extensional/shear-extensional fracture mesh composed of NNE-SSW, ESE-WNW, and NW-SE trending, high-angle faults, and fractures (Pola et al., 2014). In particular, the ESE-WNW extensional set parallels

both (i) the widest and longest fissure deforming a travertine mound in the northern part of the EuGF and (ii) the principal direction of the anisotropy derived from the variographic analysis of thermal aquifer transmissivity interpreted as a preferential groundwater flow path (Fabbri, 1997). The principal faults within the ramp show a throw of tens of meters affecting both the geological and the hydrogeological settings.

1.2. The Euganean Geothermal System: A Multiscale Conceptual Model

The results of the physical, chemical, and isotopic analyses on Euganean thermal waters (Gherardi et al., 2000; Mayer et al., 2015; Norton & Panichi, 1978) can be summarized as follows: (i) temperatures of 63 to 87 °C, near-neutral pH and salinity of up to 6 g/L; (ii) main components of Cl^- and Na^+ (70 wt%) and secondarily SO_4^{2-}, Ca^{2+}, Mg^{2+}, HCO_3^-, and SiO_2; (iii) ^{18}O and ^{2}H ratios in the range of the global meteoric water line but more negative than those of local meteoric water; (iv) an absence or very low contents of ^{3}H; (v) $^{3}He/^{4}He$ ratio (0.073–0.13) of predominantly crustal origin enriched slightly by Euganean volcanic rocks; and (vi) a variable content of Ra-Rn isotopes depending on the rising path of the water and its interaction with the bedrock. The Euganean waters have some geochemical and isotopic similarities with the lukewarm waters of the springs at the foot of the Berici hills that show lower salinity and a predominant Ca-SO_4 facies. This suggests a regional geothermal system characterized by different emerging points. The fluids show a progressive increase of Na^+ and Cl^- contents reflecting an increasing "maturity degree" of the manifestations. Their Na/Cl ratio close to the unity points to an interaction with aquifer rocks with almost constant Na/Cl ratios (Gherardi et al., 2000), as generally observed in thermal systems in carbonates (e.g., Blasco et al., 2017; Cuoco et al., 2017; Yang et al., 2017). In addition, the interaction with evaporites is suggested by (i) the relatively high content of SO_4^{2-} in Berici waters and their chemical type and (ii) the Ca/SO_4 ratio of Euganean waters (0.4–0.5) being very similar to the gypsum-anhydrite reference value (~0.42). These geochemical features evidence a long-lasting circulation and the interaction of the Euganean waters with limestones, dolostones, and evaporites (Gherardi et al., 2000). These characteristics were corroborated by the isotopic content of the Euganean travertine (Pola, Gandin, et al., 2014) showing (i) positive $\delta^{13}C$ acquired during the prolonged interaction with marine carbonates, (ii) extremely low U content typical of a deep circuit, where reducing conditions favor its precipitation (Bourdon et al., 2003), and (iii) $^{234}U/^{238}U$ activity ratio (~2) higher than unity that is typical of travertines associated to hydrothermal systems with long circulation paths at depth (Brogi et al., 2010, 2012). These water-rock interactions were further confirmed through geochemical modeling (Gherardi et al., 2000). Although high concentrations of Cl^- and Na^+ can be found in other hydrogeological settings (Pepin et al., 2015; Perello et al., 2001), Na-Cl type waters occur also in carbonate and evaporite reservoirs (e.g., Blasco et al., 2017; Chiodini et al., 1995; Fusari et al., 2017; Pang et al., 2018). In particular, the dissolution of dolomite favored by the water interaction with gypsum or anhydrite is a common process in aquifers containing dolostones and gypsiferous layers (e.g., Frondini, 2008; Goldscheider et al., 2010; Gunn et al., 2006). The geochemical results were integrated with the regional and local geological and hydrogeological settings of the study area into the EuGS multiscale conceptual model.

Stable isotopes analyses point to a meteoric origin of the thermal waters and to a recharge area elevation of approximately 1,500 m above sea level (a.s.l.). Comparable values are found in the Veneto Prealps. Since the sector toward the west does not show favorable geological conditions, reliefs along and east of the mountainous part of the Schio-Vicenza fault represent the recharge area of the system (Figure 2a). The deep infiltration of precipitation is enhanced by fractures and karst conduits, and it is mostly drained by the spring system located at the base of the relief. The remaining portion recharges both alluvial and deep rocky aquifers. The hydrogeological mass balance of the area (Aurighi et al., 2004) points to a potential flow rate of 276×10^6 m^3/year, which is sufficient to supply the volume of exploited thermal waters.

Once infiltrated, the water flows southward mostly within Mesozoic carbonate formations (Figure 2a). These formations host thermal aquifers beneath the EuGF, and they crop out into the recharge area, exhibiting good continuity along the thermal system. The damage zone of the Schio-Vicenza fault represents the main flow path of the thermal water. It consists of a complete set of Riedel-type faults as observed in synthetic sinistral strike-slip faults deforming the eastern sector of the Lessini and Berici Mountains. Local fracturing increases permeability field, favoring both a southward horizontal flow in the reservoir and a secondary vertical flow in the underlying Permian-Triassic clastic-evaporitic formations.

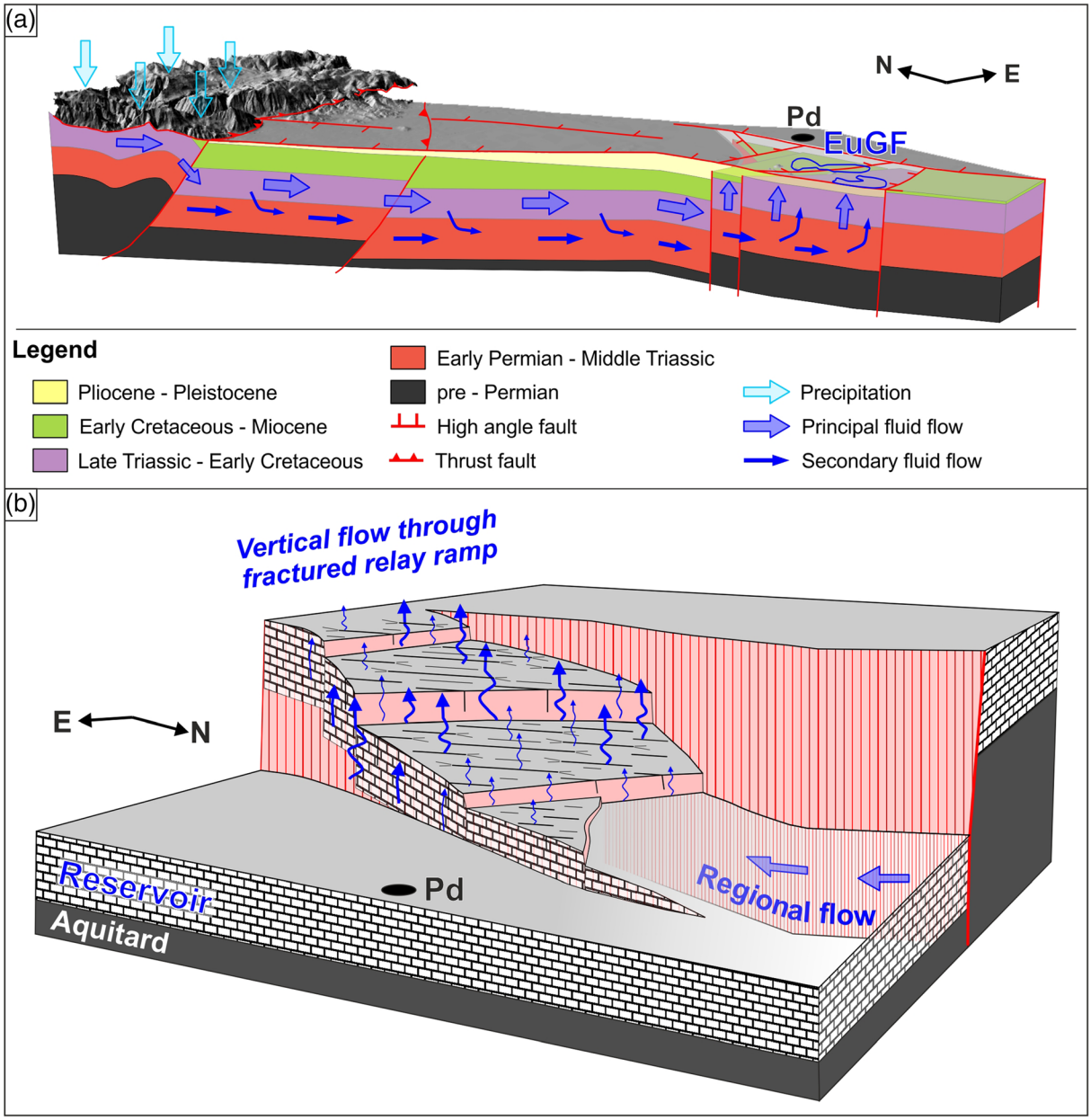

Figure 2. Three-dimensional regional (a) and local (b) conceptual models of the EuGS. The water infiltrates and flows southward mostly within the Late Triassic-Early Cretaceous carbonate reservoir. The regional flow, enhanced by the damage zone of the high-angle Schio-Vicenza fault, intercepts the fracture network of the relay ramp, favoring the rise of thermal water in the EuGF. Padua (Pd) is reported as a representative location since the sketches are not to scale.

The regional flow intersects the favorably oriented fracture mesh of the SVFS relay ramp (Figure 2b). The thermal fluids rise from the deep reservoir through the ESE-WNW trending extensional fractures and flow horizontally into highly fractured layers located at different depths. Their intensive fracturing was observed through cores and geophysical logs (Antonelli et al., 1993). The deeper aquifer is hosted by Late Triassic-Middle Jurassic carbonates at depths of 600 to 1,000 m. Having been investigated from few wells, its hydrogeological setting is only partially identified. The most investigated and exploited aquifer is found at depths of 300 to 600 m within Late Jurassic-Early Cretaceous limestones. Its transmissivity generally ranges from 100 to 600 m^2/day, although lower and higher values were locally measured (Fabbri, 1997). Locally, the water can rise up to shallow depths reaching the surface and clustering to form thermal springs. Shallow thermal aquifers are found in laterally discontinuous sandy layers of the alluvial cover, but they have not been exploited since the 1980s (Fabbri et al., 2017). Few principal areas of deep fluids rising are postulated

by the temperature and the isotopic content of the water. The upwelling from the deep reservoir is likely to be relatively rapid because the highest temperatures measured in the EuGF wells approach temperatures into the deep reservoir. Geothermometers based on K/Mg and SiO_2 evidence a reservoir temperature of 80–100 °C, while isotopic fractionation between CO_2 and CH_4 points to 170–245 °C (Gherardi et al., 2000).

This multiscale conceptual model evidences that fracture meshes associated to the SVFS and the relay ramp drive the regional to local fluid flow (Figure 2). Preferential convective water motion induced by fracturing could represent one of the principal processes warming the water. Slightly high regional crustal heat flow (70–80 mW/m^2; Pasquale et al., 2014b) and radiogenic magmatic bodies of the Euganean area (Tositti et al., 2017) could act as an extensive source of its heating. The thermal water likely has a residence time of some thousands of years as suggested by ^{14}C measurements (Boaretto et al., 2003). Such a travel time allows for long water/rock interaction that increases water salinity.

2. Methods

2.1. Governing Equations

In running coupled fluid flow and heat transport models, we relied on the FEFLOW code (Diersch, 2014). FEFLOW is a Finite Element-based simulator used to solve for flow and transport processes occurring in (un)saturated porous and fractured media with the presence of local discontinuities as represented by discrete fault zones and local fractures. Basic equations describing fluid flow and heat transport in these media are derived on the basis of conservation laws for fluid mass (equation 1), momentum (here linearized in terms of Darcian flow, equations 2 and 3), and thermal energy (equation 5). Under Boussinesq approximation, the mass conservation for the fluid phase is given by (Diersch, 2014):

$$(\rho\phi)\frac{\partial p}{\partial t} + \nabla\cdot(\rho q) = 0 \tag{1}$$

with ρ denoting fluid density, p denoting pore pressure, ϕ denoting the porosity of the porous medium, and q denoting fluid velocity. Source and sink of the fluid are neglected.

Under laminar flow conditions, groundwater flow obeys Darcy's law as follows:

$$q_i = -\frac{k_{ij}}{\mu}(\nabla_i p + \rho g\cdot\nabla z) \tag{2}$$

where k_{ij} is the permeability tensor, μ is dynamic viscosity, and g is gravitational acceleration.

Equation 2 is cast in terms of pore pressure as a primary variable. However, FEFLOW solves for equivalent hydraulic head, $h = \frac{p}{\rho g} + z$, thus leading to the following form of the momentum equation:

$$q_i = -K_{ij}\left(\nabla h + \rho^{'}\nabla z\right) \tag{3}$$

where $K_{ij} = \frac{\rho g k_{ij}}{\mu}$ is the hydraulic conductivity tensor of the porous medium and $\rho^{'} = (\rho - \rho_0)/\rho_0$ is the ratio of fluid density, which is used here to account buoyancy-driven flow in the equation.

Assuming the fluid to be the only compressible phase, mass conservation (equation 1) can be rewritten in terms of hydraulic head, which under isothermal conditions reads as follows:

$$\phi S_h\frac{\partial h}{\partial t} + \nabla\cdot(\rho q) = 0 \tag{4}$$

where $S_h = S_0 h + \varepsilon_e = \rho g\beta$ is the storativity of the medium with S_0 denoting the specific storativity, ε_e denoting the specific yield, and β denoting fluid compressibility.

Assuming the presence of thermal equilibrium between the fluid and solid phases and neglecting any variations in fluid density and porosity, thermal energy conservation yields the following heat transfer equation:

$$(\rho c)_b \frac{\partial T}{\partial t} - \nabla \cdot \left(\lambda_b \nabla T - \rho c_f q T \right) - H = 0 \quad (5)$$

where $(\rho c)_b = \phi \rho_f c_f + (1-\phi)\rho_s c_s$ and $\lambda_b = \phi \lambda_f + (1-\phi)\lambda_s$ are the volumetric heat capacity and thermal conductivity of the bulk medium, T is temperature, and H is a source term taking radiogenic heat production into account in our formulation. Subscripts f and s represent the fluid and the solid phases, respectively.

Equations 1, 4, and 5 are finally coupled by setting a functional form behavior for fluid density and viscosity as depending on the respective primary variable of the problem. For the specific problem at hand, fluid viscosity is kept constant while the density of the fluid varies linearly with temperature, following $\rho = \rho_0(1 - \alpha \Delta T)$ with α being the volumetric thermal expansion coefficient of the fluid.

2.2. Model Setup and Boundary Conditions

2.2.1. Geological Reconstruction and Model Discretization

The aim of the numerical model is to simulate the fluid flow driven by small-scale fractures and mesoscale faults within the Schio-Vicenza fault damage zone and the relay ramp reproducing the natural condition of the EuGS before the forced exploitation of the thermal resource by wells. The explicit discrete fracture approach superimposing discrete elements (DE) to an equivalent porous medium was employed. This approach reproduces fracture networks at different scales (Bundschuh & Suárez Arriaga, 2010), and it is used to simulate fluid flow and heat transport in fractured media such as hydrothermal systems (Cherubini et al., 2013; Scheck-Wenderoth et al., 2014). The main faults involved in the EuGS were modeled by 2-D DE using the Darcy law for fluid motion. Fractured bedrocks in the damage zones and relay ramp and the undeformed protolith were modeled as equivalent porous medium.

The modeling domain extended over central and outflow parts of the EuGS (Figure 3a). The outflow area was located at the center of the domain to avoid boundary effects on the distributions of primary variables. The relay ramp is approximately 20 km long and 11 km wide with an aspect ratio (i.e., the ratio between length and width) consistent with literature values between 1 and 10 over a wide range of scales (Fossen & Rotevatn, 2016). The domain was extended 7.5 km east, reproducing the average distance between the Conselve-Pomposa and Travettore-Codevigo faults along the ramp, and 30 km north, reaching the foot of the Prealps. Similar buffers were imposed westward and southward. The final extent was set to 80 km × 26 km in plain view, and the height was set to 5 km based on the maximum thicknesses of the sedimentary units (Figure 3b). The top of the domain was set at sea level since the altitude of ground surface decreases from 50 m to 0 m a.s.l.

The domain was divided into three blocks separated by sharp discontinuities (Figures 3b and 3c), reproducing respectively the main structural domains of central Veneto and the fault zones of the regional faults (i.e., fault core and damage zone). The fault zones were simplified with N-S trending vertical geometries, and their thicknesses were set to 0.5 km using an empirical correlation with the fault displacement (Savage & Brodsky, 2011) obtained by seismic sections in the study area (Pola, Ricciato, et al., 2014). Although the SVFS likely deforms deep parts of the crust, the modeled fault zones ranged from the top of rocky hydrostratigraphic units to 4.6 km below ground level (b.g.l.), avoiding contact with the boundary conditions (BC) at the base of the domain and potential numerical issues. Despite the simplified architecture, this reproduction is suitable for a regional numerical model designed to simulate the processes developing the EuGS. This faults representation slightly changes their relative orientations in relation to the regional fluid flow, but it does not affect their conduit behavior favored by the dense fracturing in the fault zones. The fault zones thicknesses could be a further relevant simplification. Local data are lacking, and employing a well-established correlation with the fault displacement, which covers various geological settings and scales, was the best choice. Furthermore, their importance as preferential flow paths is mostly controlled by their hydrogeological properties, which were increased from the values of the protolith (section 2.2.2).

Formations of the study area were grouped into five hydrostratigraphic units (Table 1). In particular, the Late Triassic-Early Cretaceous hydrostratigraphic unit represented limestones and dolostones constituting the reservoir. Standard hydrostratigraphic sequences were constructed for each block using outcrop data and stratigraphic logs. The units were modeled as horizontal layers due to their moderate southward deepening in the modeled area relative to their thickness. The result was the eastward subsiding of hydrostratigraphic units (Figure 3d) reproducing the regional geological setting (Figure 1b).

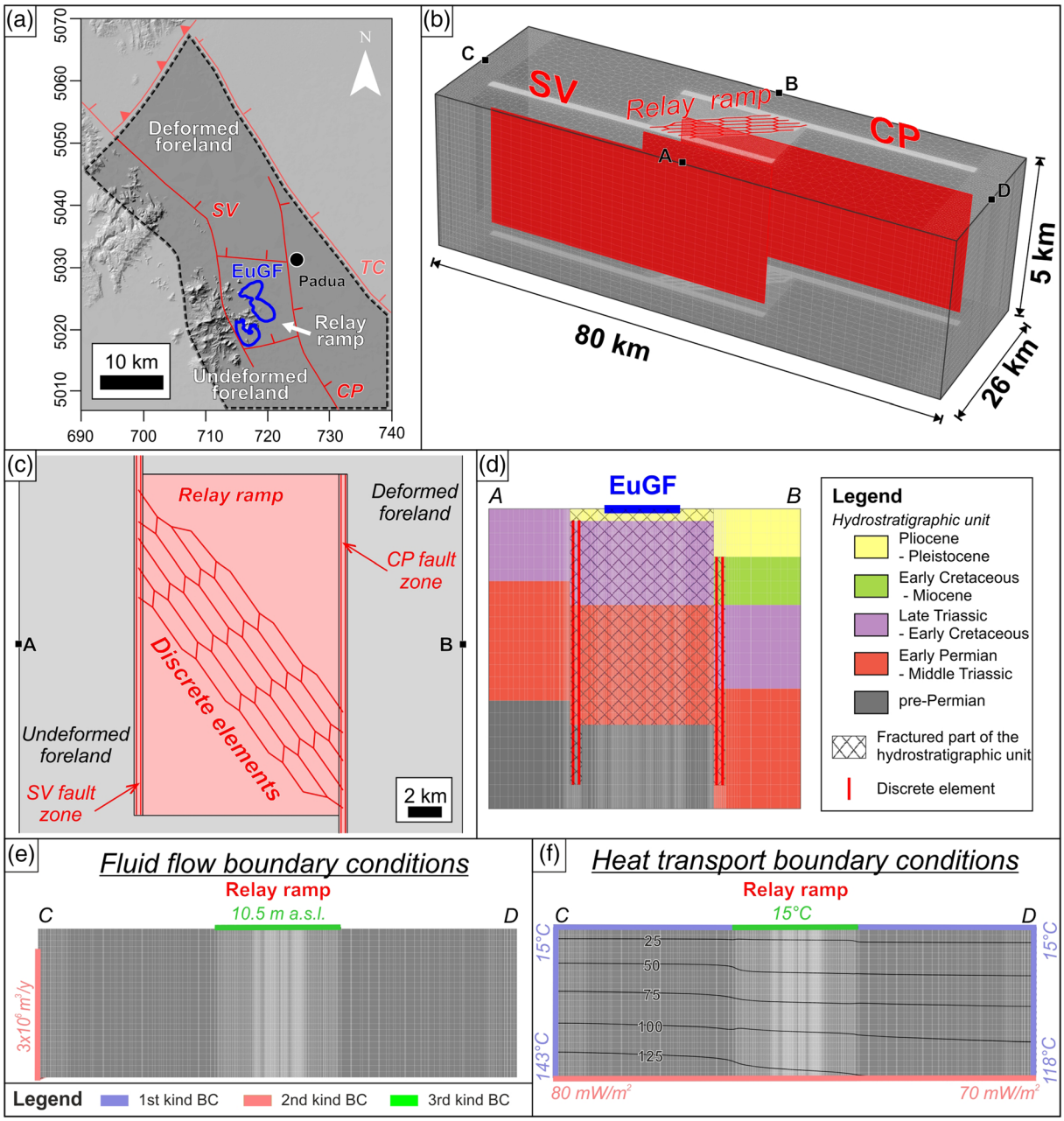

Figure 3. Setup of the numerical model. The modeled area (dashed polygon in a) was outlined to include the main regional fault segments (SV: Schio-Vicenza fault; CP: Conselve-Pomposa fault; TC: Travettore-Codevigo fault) and their relay ramp. Their geometries were schematized and implemented into a numerical model (b). The model reproduced the structural domains of central Veneto (c), and it was discretized into five hydrostratigraphic units (d, vertical exaggeration 5:1). The fractured parts of the units (i.e., fault zones and relay ramp) were distinguished from the undeformed protolith using different parametrizations (Table 1). Discrete elements (c; Table 2) were superimposed to the fractured zones simulating regional and local faults. Fluid flow and heat transport boundary conditions (BC in e and f, respectively) and initial conditions of temperature distribution (black contour lines in f) completed the model.

Two N-S trending DE were implemented within both fault zones, while the fracture mesh deforming the EuGF subsurface was modeled by three sets of DE (Figure 3c and Table 2). Since the bounding faults were rotated 30° clockwise to obtain the N-S trend, the directions of the local fractures were accordingly reoriented. The resulting network of DE connected the bounding faults and extended from the surface to 4 km b.g.l. The average widths of fracture sets measured on the Euganean travertine deposit (Pola, Gandin, et al., 2014) were decreased by 1 order of magnitude to obtain the width of the corresponding DE (d in Table 2).

Table 1
Physical Parameters (Units Shown in Brackets) Assigned to Undeformed and Fractured Parts of the Hydrostratigraphic Units (Protolith and Fractured Rock, Respectively)

		1	2	3	4	5
	Time	Pliocene-Pleistocene	Early Cretaceous-Miocene	Late Triassic-Early Cretaceous	Early Permian-Middle Triassic	Pre-Permian
Unit	Lithology	Sand, clay, silt	Marl, limestone, sandstone	Limestone, dolostone	Clastic and volcanic rocks, limestone, anhydrite	Phyllite, schist
K_h (ms^{-1})	Protolith	1.00E−08	1.00E−09	4.00E−08	8.00E−09	1.00E−10
	Fractured rock	1.00E−06	1.00E−07	4.00E−06	8.00E−07	1.00E−08
K_h/K_v (−)	Protolith	100.00	100.00	100.00	100.00	100.00
	Fractured rock	10.00	10.00	10.00	10.00	10.00
ε_e (%)	Protolith	4.00	6.00	5.00	5.00	1.50
	Fractured rock	29.00	31.00	30.00	30.00	26.50
S_0 (m^{-1})	—	2.00E−07	2.00E−07	2.00E−07	2.00E−07	2.00E−07
φ (%)	Protolith	14.00	16.00	15.00	15.00	11.50
	Fractured rock	39.00	41.00	40.00	40.00	36.50
ρc ($MJ\ m^{-3}\ K^{-1}$)	—	1.90	1.80	2.20	2.00	3.00
λ ($W\ m^{-1}\ K^{-1}$)	—	3.00	3.00	4.00	3.50	4.50
H (μWm^{-3})	Protolith	0.00	0.50	0.50	0.50	2.00
	Relay ramp	0.00	—	1.50	0.50	2.00

Note. Their principal lithologies and ages are reported. K_h: horizontal hydraulic conductivity; K_h/K_v: anisotropy conductivity ratio (horizontal versus vertical hydraulic conductivity); ε_e: specific yield; S_0: specific storativity; ϕ: total porosity; ρc: volumetric heat capacity; λ: thermal conductivity; H: radiogenic heat.

The model domain was discretized using a prismatic mesh that was refined within the fault zones and relay ramp. The vertical extent was divided into 25 layers of 200 m thick, allowing to reproduce average thicknesses of the hydrostratigraphic units and fault throws. The resulting mesh consisted of 2,693,775 elements.

2.2.2. Hydraulic and Thermal Properties

Measurements carried out in both the EuGF and the central Veneto, integrated by literature collections, were used to define hydraulic and thermal properties of the hydrostratigraphic units (Table 1) and DE (Table 2). The parametrization of undeformed and fractured parts of the units (protolith and fractured rock, respectively, in Table 1) and of the DE was differentiated to reflect their role in the EuGS.

K_{ij} (equation 3) was simplified by considering the tensor as orthotropic, and horizontal and vertical hydraulic conductivities (K_h and K_v, respectively) corresponding to K_x and K_y and to K_z were used. The hydraulic conductivity of the EuGF reservoir was investigated through aquifer tests of approximately 40 wells (Fabbri, 1997). The lowest value of its distribution was used as K_h of the fractured Late Triassic-Early Cretaceous hydrostratigraphic unit, which reproduces the reservoir (Table 1). The K_h of the other

Table 2
Physical Parameters (Units Shown in Brackets) Assigned to the Discrete Elements

		1	2	3	4
	Location	Relay ramp	Relay ramp	Relay ramp	Fault zone
	Direction	N145°E	N125°E	N185°E	N-S
Discrete elements set	Kinematics	Extensional	Strike slip	Strike slip	Transtensional
d (m)		0.04	0.02	0.02	0.04
K (ms^{-1})		5.00E−03	1.00E−03	1.00E−03	5.00E−03
S_0 (m^{-1})		2.00E−05	2.00E−05	2.00E−05	2.00E−05
φ (%)		100.00	100.00	100.00	100.00
ρc ($MJ\ m^{-3}\ K^{-1}$)		3.00	3.00	3.00	3.00
λ ($W\ m^{-1}\ K^{-1}$)		4.50	4.50	4.50	4.50

Note. Their location and the kinematics of the corresponding fracture sets are reported. d: aperture; K: hydraulic conductivity; S_0: specific storativity; ϕ: total porosity; ρc: volumetric heat capacity; λ: thermal conductivity.

hydrostratigraphic units were established by literature data sets (e.g., Domenico & Schwartz, 1998). The K_h in their fractured parts (i.e., fault zones and relay ramp) was set 2 orders of magnitude higher than the undeformed protoliths, corresponding to permeability ratios between deformed and undeformed rocks (Bense et al., 2013; Faulkner et al., 2010). The K_v was calculated from the K_h using different K_h/K_v ratios for fractured and undeformed parts of the domain (Table 1). The hydraulic conductivity of the DE (K) was also obtained from the experimental distribution. Since the measurements investigated both rock and fractures, the mean and maximum values were increased by 1 order of magnitude and applied to the strike-slip and extensional DE, respectively. The regional DE were modeled using the same K of the extensional DE (Table 2). Similarly, the S_0 (equation 4) was obtained from the aquifer test results. The minimum was used as the value of the hydrostratigraphic units (Table 1), while the maximum was set for the DE (Table 2).

Literature data sets (Pasquale et al., 2011; Vosteen et al., 2003; Vosteen & Schellschmidt, 2003) were used to calculate the ε_e, ϕ, ρc, and λ (equations 4 and 5) based on the main lithologies of the units. The ε_e and ϕ of the fractured rock were increased by 25% accounting secondary porosity induced by the fracturing. The ϕ of DE was set to 100%, while the ρc and λ was set as equal to the highest values of the hydrostratigraphic units.

High levels of radioactive elements in volcanic rocks of the Euganean Hills and their contributions to the temperature increase in the EuGF were modeled by the radiogenic heat source (H in equation 5). Representative H values were calculated for the sedimentary, metamorphic, and volcanic lithologies (0.5, 2, and 3 $\mu W/m^3$, respectively) using Uranium, Thorium, and Potassium concentrations and densities of the rocks in Veneto (Faccenda et al., 2007; Germinario et al., 2017; Strati et al., 2015; Tositti et al., 2017). The H values of the sedimentary and metamorphic rocks were applied to rocky sedimentary and pre-Permian hydrostratigraphic units, respectively. The volcanic bodies were simulated by increasing the H of the Late Triassic-Early Cretaceous hydrostratigraphic unit in the relay ramp (Table 1) since their maximum depth is 1 km (Norinelli, 1979). Such increase was calculated using the percentage of volcanic rock obtained by stratigraphic logs (40%).

2.2.3. Initial and Boundary Conditions

Equations 1 to 5 represent an initial and boundary value problem. Its solution requires the definition of proper sets of boundary conditions (BC) both for hydraulic and thermal components of the discrete problem and of initial distributions for the primary variables (hydraulic head and temperature).

The fluid flow BC (Figure 3e) were set as Neuman-type (second kind) BC of the northern border of the domain and Cauchy-type (third kind) BC of the top in the relay ramp. The second kind BC reproduced the flow from the recharge area. An inflow of 3×10^6 m^3/year was applied to rocky hydrostratigraphic units of the foredeep. The inflow value was obtained after calibration, and it produced a hydraulic head of 600 m to 900 m a.s.l. on the northern part of the reservoir. Although this range was lower than the actual elevation of the infiltration zone (1,500 m a.s.l.), it accounted for the loss of hydraulic head from the recharge area to the foot of the Prealps (i.e., northern boundary of the model). The third kind BC reproduced the occurrence of the Euganean thermal springs, and it was described as a hydraulic head of 10.5 m a.s.l. corresponding to the mean elevation of the EuGF. Furthermore, it required inflow and outflow transfer coefficients. A constraint condition inhibited the inflow, while the outflow coefficient was set as numerically equal to the K_v of the Pliocene-Pleistocene hydrostratigraphic unit and to the K divided by the aperture, d, for the DE (Table 2). The constraint condition both favored the outflow and inhibited the infiltration of local surficial waters into the thermal aquifer, which can be excluded considering the isotopic contents of the thermal waters.

The heat transport BC (Figure 3f) were set as Dirichlet-type (first kind) BC of the northern and southern borders of the domain and of the top, Cauchy-type (third kind) BC of the top in the relay ramp, and Neuman-type (second kind) BC of the base. A prescribed value of 15 °C was set for the first kind BC of the top, representing the average annual temperature, while it was set as equal to the initial temperature distribution at the northern and southern borders. The second kind BC reproduced the heat flow from the lower part of the crust, and it decreased southward from 80 to 70 mW/m^2 (Pasquale et al., 2014b). The temperature of the third kind BC was 15 °C as the first kind BC. Inflow and outflow transfer coefficients were calculated using the same approach used for the fluid flow coefficients.

The initial hydraulic head was set to 0 m a.s.l., while the initial distribution of temperature was obtained from a preliminary steady-state simulation (Figure 3f). Its BC included Dirichlet-type (first kind) BC at the top of the domain and Neuman-type (second kind) BC at the base. The same BC values were applied.

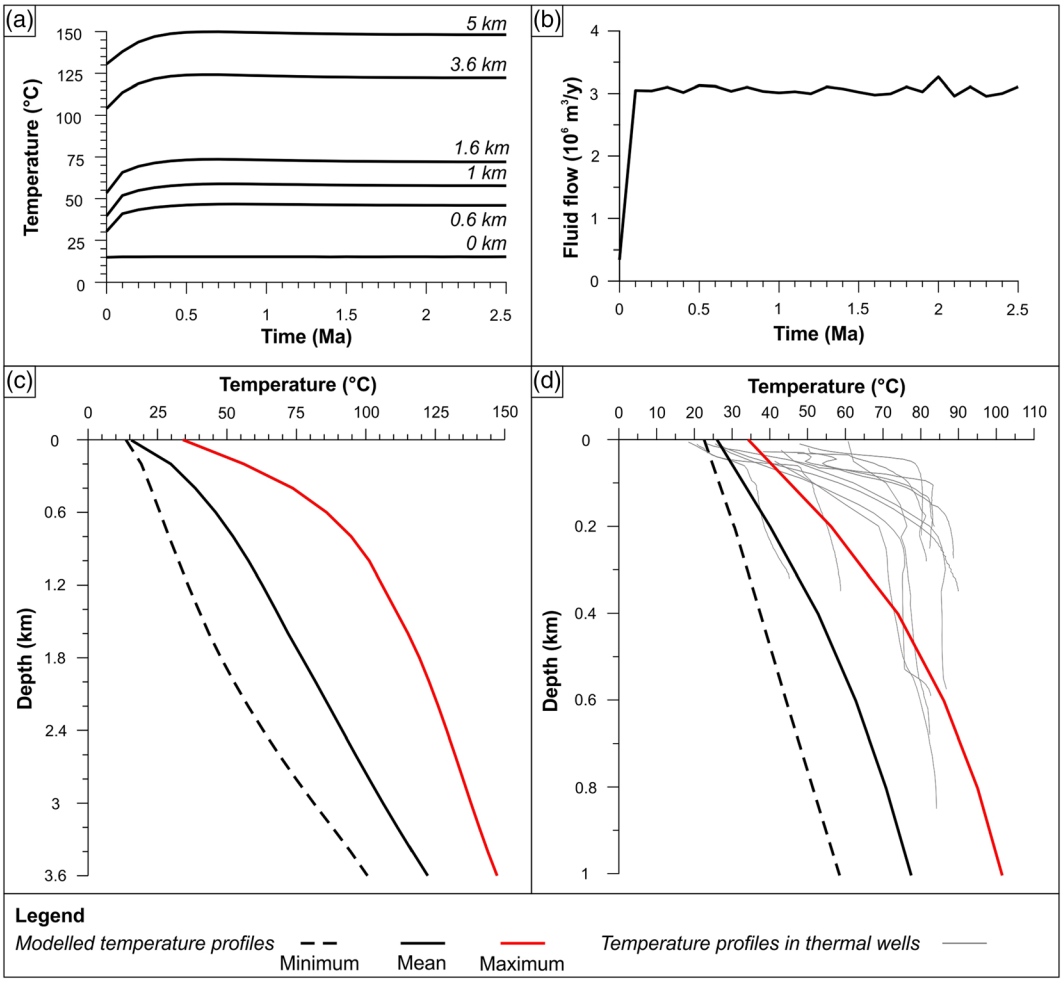

Figure 4. Slight variations in the mean temperature (a) and outflow (b) observed over time in the relay ramp suggest that their final distributions reproduce the natural state of the system. The final temperature (c) is detailed with temperature profiles within the simulated thermal anomaly (Table 3), which are compared to the measurements of the EuGF wells (d).

The described features were tested in a transient simulation for a period of 2.5 Ma to achieve a quasi steady state solution. This simulation was obtained after many tests with different sets of parameters and hereafter is referred to as the reference simulation. Further subsidiary simulations were performed to assess the impact of regional and local faults and radiogenic heat production on the temperature distribution. The obtained results are presented and compared to available local and regional temperature distributions and flow rate.

3. Results

3.1. Reference Simulation

The initial temperature distribution within the relay ramp obtained through the steady-state simulation ranges from 15 to 139.5 °C. Temperature generally increases from these initial values, reaching approximately stable conditions after 1 Ma (Figure 4a). Similarly, the volume of water flowing out from the third kind BC of the relay ramp varies slightly over time (Figure 4b). Therefore, the obtained solution is of a quasi steady state reproducing the natural conditions of the system before the exploitation of the thermal waters by wells. The final temperature distribution within the relay ramp was investigated through temperature profiles and maps at different depths. The maps show that the temperatures are lower in the southern part of the relay ramp (Figure 5) where a slight decrease from the initial distribution occurs. The lowest values (minimum temperature profile in Figure 4c) are modeled in the southern part of the Schio-Vicenza fault zone. On the

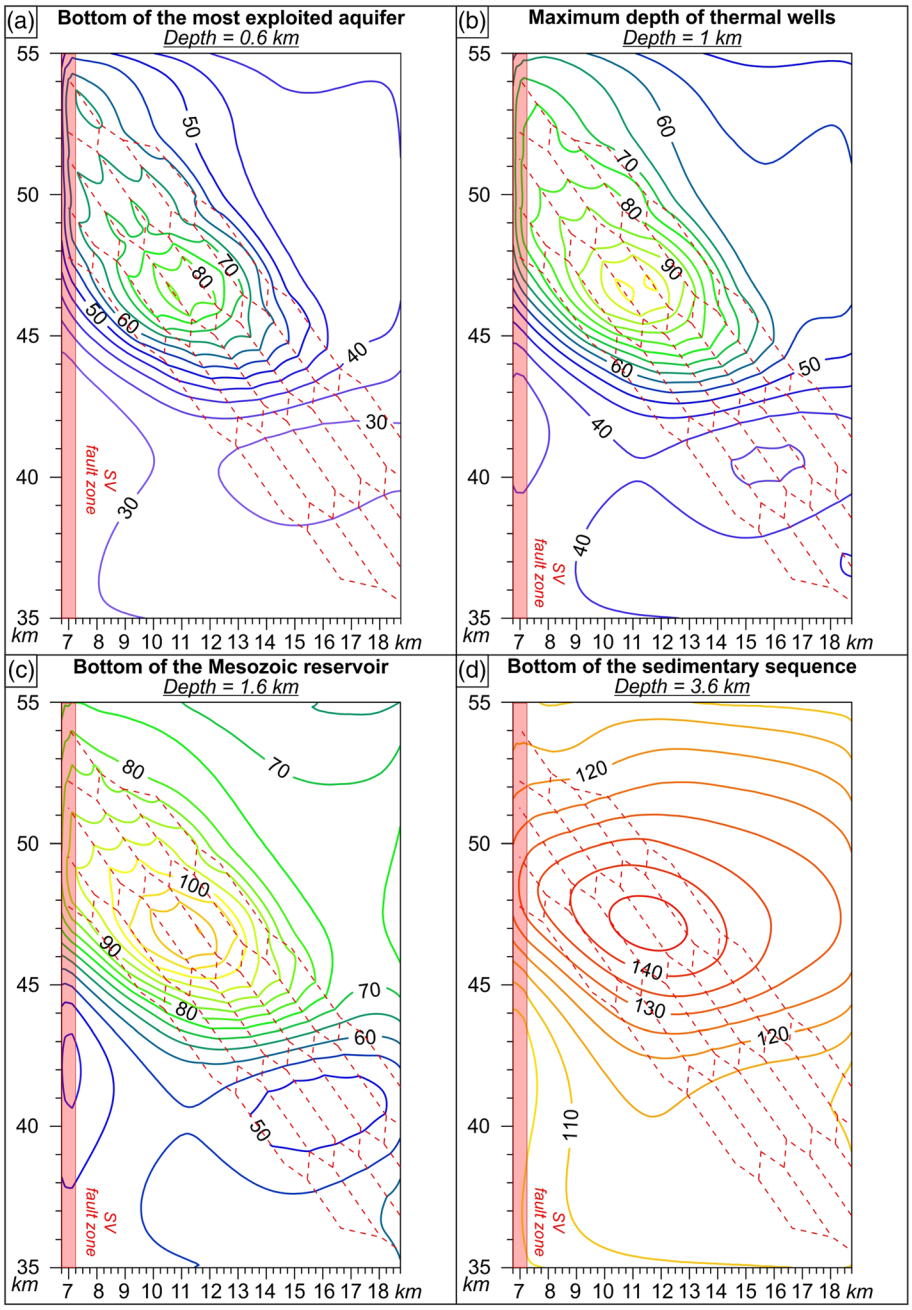

Figure 5. Maps of the temperature (in °C) modeled in the relay ramp at different depths. Discrete element mesh deforming the ramp (dashed lines) and the southern part of the Schio-Vicenza (SV) fault zone are also shown.

other hand, an increase from the initial steady-state condition is observed in northern and central parts of the ramp. This results in the formation of a positive thermal anomaly enclosed by isotherms corresponding to the average modeled temperature (mean temperature profile in Figure 4c). Isotherms follow a general NW-SE trend in the upper part of the domain. This trend parallels the network of DE implemented within the relay ramp modeling domain, which simulates the fracture mesh deforming the bedrock. Furthermore, isotherms exhibit an irregular shape produced by local temperature increases (Figures 5a, 5b, and 5c) along the widest and highest permeable DE, which reproduce the extensional open fractures. The isotherms shift to a regular ellipsoidal shape at greater depths with a prevalent E-W trend (Figure 5d).

Table 3
Temperature Distribution in the area of the Relay Ramp Showing an Increase Higher Than 50% From Initial Values

		Temperature (°C)		
	Depth (km)	Minimum	Mean	Maximum
0.00	Top of the domain	22.5	25.9	34.1
0.20	Top of the rocky units	30.4	39.9	56.1
0.60	Bottom of the most exploited aquifer	44.2	62.6	85.9
1.00	Maximum depth of thermal wells	58.3	77.2	101.2
1.60	Bottom of the Mesozoic reservoir	79.0	93.8	115.2

Within the simulated thermal anomaly, the increment from the initial condition is approximately 50% to 150% in the reservoir and 25% to 75% in the underlying hydrostratigraphic unit. The part of the domain showing a temperature increase higher than 50% was selected to numerically detail the obtained results. Its extent is approximately 70 km^2 until the depth of 1 km, and it is comparable to that one of the thermal anomaly southwest of Padua including the EuGF and its hinterland with lukewarm waters (Antonelli et al., 1995). The extent progressively decreases until 3 km in depth where the temperature increase is lower than 50%.

The simulated values in the rocky reservoir (Table 3) were compared to field data from the EuGF. First, temperature profiles were considered (Figure 4d). These measurements were conducted in wells where the exploitation was temporarily stopped from a few hours to several days. Despite comparable surficial temperatures, the trends of the simulated and experimental profiles differ at shallow depths. The simulated temperatures are generally lower than well profiles showing a sharp temperature increase. At greater depths (approximately below 0.5 km), the observations and the modeling results are comparable. The bottom hole temperatures of the deepest profiles were measured as 82.6, 82.4, and 84.2 °C at depths of 590, 680, and 850 m, respectively. Furthermore, 92 °C at a depth of 1 km was inferred from the results of a partial thermal log investigating the deepest artesian well of the EuGF. These values are within the modeled range of temperatures at comparable depths (Table 3).

The discrepancy found at shallow depths can be explained by considering that the simulation and the observations are representative of different thermal and hydraulic conditions. The simulation reproduces the natural, quasi-static state of the EuGS that was the state before any forced extraction of the waters. By contrast, the measurements have been conducted under dynamic conditions and they should be considered as still being affected by the prior exploitation. The effect of the exploitation on the well profiles has been corroborated by the results from a 1-D model as detailed in the supporting information to this manuscript. The 1-D model, run with the GOLEM simulator (Cacace & Jacquey, 2017), simulated the temperature variations in an ideal well of the EuGF during the extraction and the subsequent shut-in period. Starting from the natural undisturbed thermal regime (i.e., the distribution resulting from the regional model), the model reproduced the trends of the EuGF temperature profiles and it evidenced a long-lasting impact of the well activity on the subsurface temperature.

The analysis of the regional modeling results was completed by considering the wellhead temperatures measured during chemical surveys and the reservoir equilibrium temperatures inferred by geothermometers (Gherardi et al., 2000; Mayer et al., 2015; Norton & Panichi, 1978). Since the shallow colder aquifers are isolated and the measurements were conducted in wells active for a few days, the wellhead temperatures should reflect the temperature in the thermal aquifer being a good indicator for the natural condition of the system. The waters exploited from the most investigated part of the rocky reservoir (up to 600 m deep) show temperatures of 48.5 to 87 °C, while the waters from its deep section (up to 1 km deep) are 63 to 85 °C. Temperatures within the simulated thermal anomaly (Table 3) are in the range of the measurements with minor discrepancies that can be explained by the extent of the available data sets. Shallow depths are poorly investigated in colder marginal parts of the thermal field, but wellhead temperatures of 25–30 °C are found in its hinterland, supporting the modeling result. Conversely, the hottest parts lack deep wells resulting at maximum wellhead temperatures lower than the simulated values. Considering the deeper part of the reservoir (1–1.6 km deep), the simulated temperatures (Table 3) are in agreement with the values inferred by K/Mg and SiO_2 geothermometers (80–100 °C). On the other hand, the performed simulation partially approaches the minimum value (170 °C) inferred through isotopic fractionation between CO_2 and CH_4 (Gherardi et al., 2000). As a matter of fact, the maximum modeled temperature is 147.2 °C at the base of the sedimentary hydrostratigraphic units (3.6 km deep) and reaches up to 168 °C at the base of the domain.

Since the reference simulation reproduces the temperatures of the EuGF, a regional analysis was performed. A temperature profile and the bottom hole temperatures of deep boreholes in northern and central parts of the Veneto plain foredeep (Figure 1a; Pasquale et al., 2013) were compared to the model results for corresponding regions of the domain. Mean temperature profiles were considered since the ranges of simulated

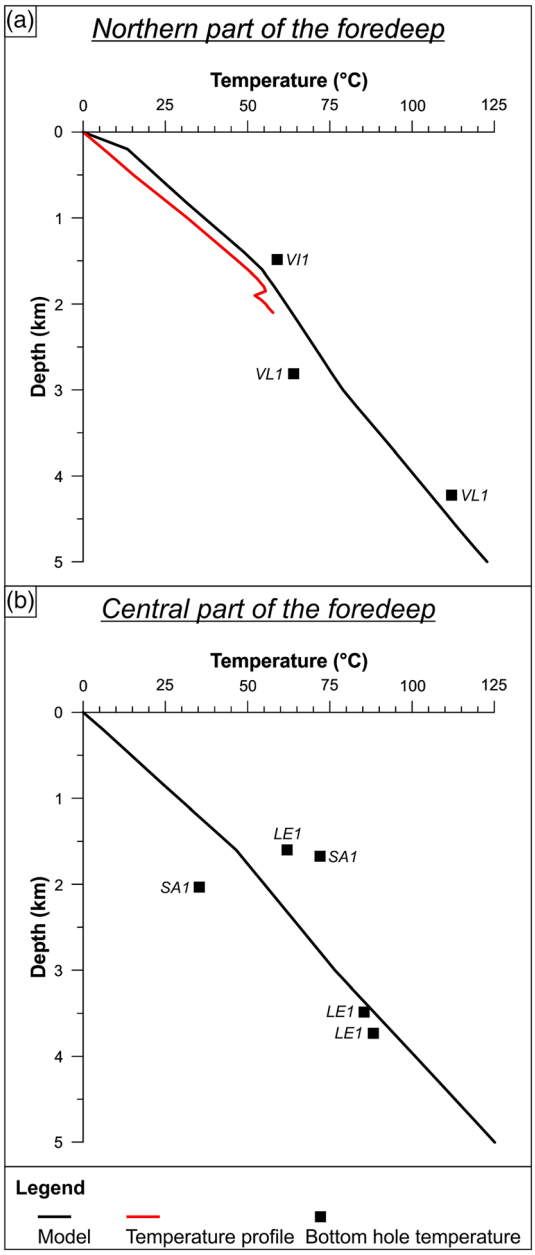

Figure 6. Normalized simulated (black lines) and measured (red line: temperature profile; square: bottom hole temperature) temperature distribution in northern (a) and central (b) parts of the foredeep. Good agreement between the values is shown. The locations of the investigated wells (VI1: Vicenza 1; VL1: Villaverla 1; LE1: Legnaro 1; SA1: Sant'Angelo di Piove di Sacco 1) are reported in Figure 1a.

values were small. The data (simulated or measured) were normalized by subtracting surficial temperatures to focus on trends. The measurements of the northern foredeep show good agreement with the reference simulation (Figure 6a). The normalized simulated temperature is 3 to 8 °C higher than the normalized temperature profile of the Vicenza 1 well, while the difference from normalized bottom hole temperatures varies from −7 to 11 °C. On the other hand, temperatures in the central foredeep show dissimilar behaviors (Figure 6b). Measurements taken from 1.6 and 2 km deep are approximately 20 °C different from the modeling results, while those from 3.5 and 3.8 km deep are approximately 5 °C lower. The discrepancy at shallow depths could be related to local heterogeneities in the hydrogeological setting (Pasquale et al., 2013), producing convective forces higher than those in the simulation.

Analyses of the temperature distributions on regional and local scales show that the reference simulation reproduces both the regional and local observations. Since the basal heat flow does not change with time (i.e., the system has a constant basal source of heat), the development of the thermal anomaly could be related to an increased convection in the relay ramp than in the protolith induced by enhanced hydraulic properties. Regional and local fluid flows were investigated to better quantify this last assertion. The reported values are averages calculated from 1.5 to 2.5 Ma within the quasi steady state of the solution (Figure 4).

The recharge of the system is represented by an inflow of 3×10^6 m^3/year (second kind BC; Figure 3e). It produces a generally southward flow in the northern domain preferentially focused across and along the highly permeable fractured zone, which reproduces the Schio-Vicenza fault zone. The range of flow velocities in the fractured part of the Late Triassic-Early Cretaceous hydrostratigraphic unit is 10^{-2} to 10^3 m/year, and it decreases by 1–2 orders of magnitude in its undeformed section. The resulting flow into the relay ramp is 1.88×10^6 and 0.98×10^6 m^3/year from the fault zone and the protolith, respectively. These inflows represent the main sources of the approximately 3×10^6 m^3/year outflowing from the top of the domain in the area of the relay ramp (third kind BC; Figure 3e). The flux within the relay ramp is highly variable. Its range is 10^{-5} to 1 m/year in the hydrostratigraphic unit of the reservoir, and it slightly decreases in the underlying unit. Flux magnitudes increase by 3–4 orders of magnitude in the DE with maxima observed in the extensional ones. The horizontal directions of flow vectors vary across the ramp, while their vertical components show a spatial pattern. An upward flow occurs in the northern and central parts where the temperatures increase with respect to the initial configuration (Figure 7). To the south, downward flow occurs resulting in a temperature decrease. These results corroborate the impact of the fluid flow on the temperature distribution in the relay ramp. The remaining parts of the domain (i.e., Lessini-Berici-Euganean block, Conselve-Pomposa fault zone, and southern foredeep) slightly influence the fluid flow in the relay ramp, showing flux magnitudes 3–4 orders of magnitudes lower than those observed in the northern region.

3.2. Subsidiary Simulations

The results of the reference simulation highlight the importance of the local geological setting of the relay ramp on the development of the Euganean thermal anomaly. Therefore, subsidiary simulations were designed to uncover the impact of both the fracturing in the relay zone and the radiogenic volcanic rocks.

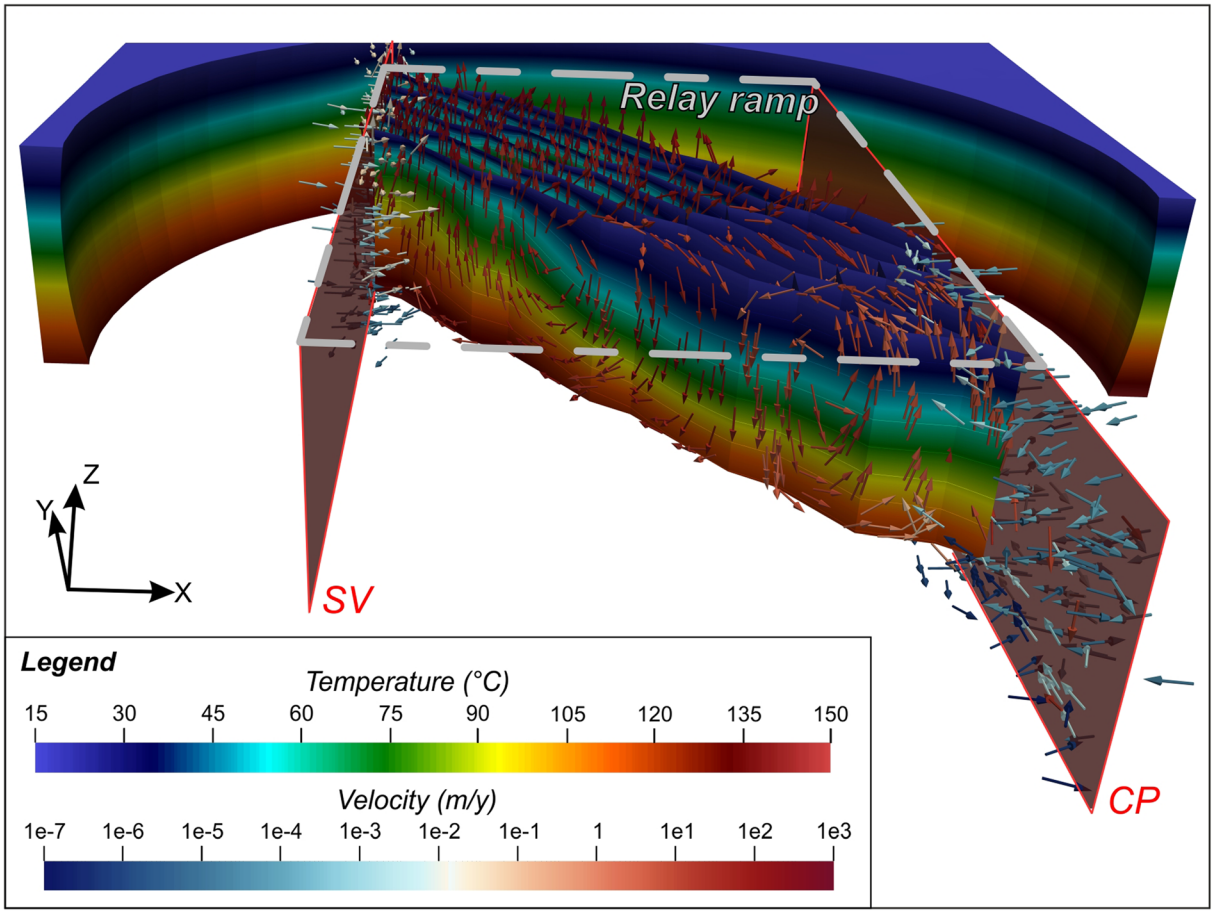

Figure 7. Temperature and fluid flow distributions of the central part of the modeling domain. The regional fluid flow increased by the fault zone of the Schio-Vicenza fault (SV) feeds a local circulation within the relay ramp, where a convective process produces temperatures higher than in the protolith (values shown as background). The fault zone of the Conselve-Pomposa fault (CP) provides a minor contribution to the local fluid flow.

The connectivity between the segments of the SVFS could be provided by a breaching fault (instead of the relay ramp), which represents the final stage of linkage between the faults bounding a relay ramp (Fossen & Rotevatn, 2016). This potential geological setting was reproduced with an approximately 500 m wide fractured zone that connected regional fault zones replacing the fractured area of the relay ramp. The breaching fault zone was considered as fractured bedrock, and DE were superimposed (Figure 8b), while the remaining part of the ramp structural domain was considered undeformed. The vertical discretization of the hydrostratigraphic units, their parametrization, and the initial and boundary conditions were kept the same as those of the reference simulation. The simulation was run for 2.5 Ma, producing a quasi steady state solution after 1 Ma. A thermal anomaly along the breaching fault zone develops in the central part of the domain (i.e., relay ramp structural domain of the reference simulation). Mean and the maximum temperatures in this area are 5 to 20 °C lower than those of the reference simulation (Figure 8a), and only the minimum values are slightly higher. A detailed analysis within the anomaly reveals temperatures from 29.6 to 73.6 °C and from 45 to 81 °C in the investigated part of the reservoir (0.2–0.6 and 0.6–1 km deep, respectively), reaching 86.9 °C at its base (1.6 km deep). Although the minima roughly correspond, the maxima are lower than both the reference simulation (Table 3) and the wellhead temperatures at the same depths. Furthermore, the simulated anomaly shows both a smaller extent than in the reference simulation (Figure 8b) and a local-scale development that is not compatible with the Euganean thermal anomaly.

The simulation assessing the impact of the radiogenic volcanic bodies was designed by applying a uniform radiogenic heat (H in Table 1) to the rocky sedimentary hydrostratigraphic units. The H was set to 0.5 μW/m^3 as the reference value calculated for the sedimentary rocks (section 2.2.2). The structural and the hydrostratigraphic settings, the parametrization (except H), and the initial and boundary conditions corresponded

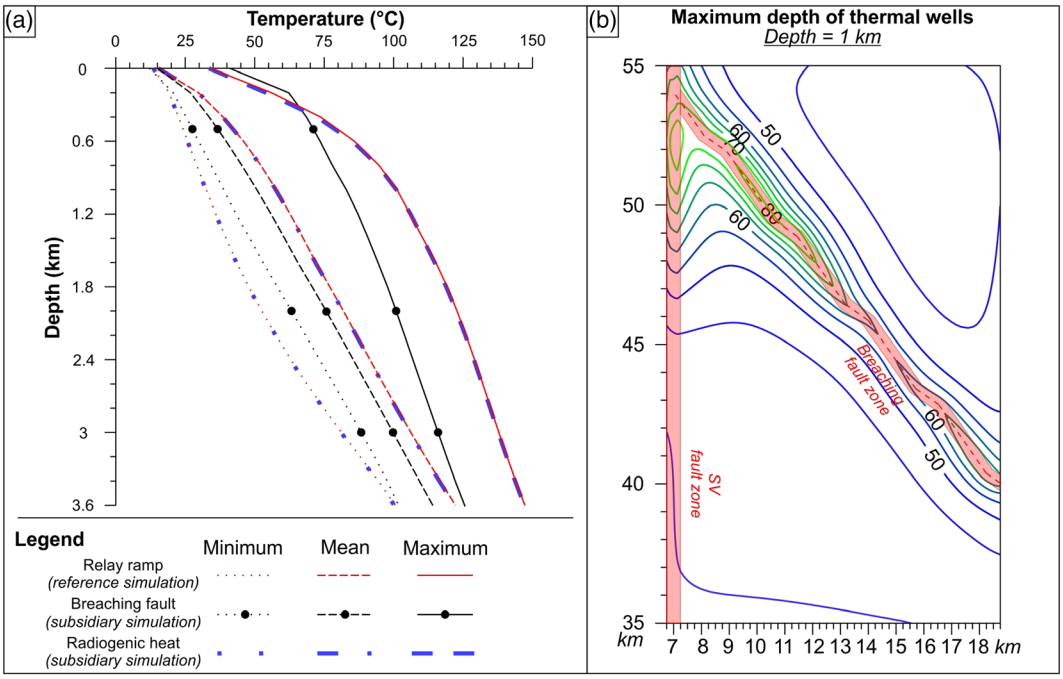

Figure 8. Temperature distributions of the subsidiary simulations in the central part of the domain are compared to values of the reference simulation (a). The simulated values are lower for the "breaching fault simulation", while the results of the "radiogenic heat simulation" are comparable. The temperature distribution resulting from the "breaching fault simulation" (b) evidences a thermal anomaly smaller and colder than that of the reference simulation at comparable depths (Figure 5b).

to the reference simulation. The simulation was run for 2.5 Ma resulting in a quasi steady state solution. The temperature distribution is comparable to the reference simulation, showing a temperature decrease of 2 °C (Figure 8a).

The importance of regional processes was also investigated through specific simulations. However, the modeled scenarios are unlikely and the corresponding results were not detailed. In particular, it is worth mentioning the scenario "without regional faults". Despite its inconsistency with structural data for central Veneto, this scenario is unlikely due to the long-lasting activity of the EuGS (at least 34 ka; Pola et al., 2011). The regional faults and their interaction are crucial to the stress accumulation in the relay ramp. This process favors the local fracturing and its maintenance over time (Curewitz & Karson, 1997), and its absence would result in a progressive clogging of the fractures and the inhibition of the water flow.

4. Discussion

The EuGS and the connected shallow thermal resource exploited in the EuGF are the result of concurring regional and local structural and hydrogeological processes. These processes are included within the renewed conceptual model of the system and are reproduced in numerical simulations. Despite the simplifications of the stratigraphic and structural settings, the performed "block-like" numerical model reproduced well the geological setting of central Veneto at regional scale (Figures 1 and 3). Based on the obtained results, it can be concluded that horizontal and vertical temperature distributions of the Euganean thermal anomaly and the regional distribution of central Veneto are reproducible in a numerical framework that accounts for first-order physical principles of fluid flow and heat transport. The highly permeable fault zone of the Schio-Vicenza fault locally increases the regional fluid flow that feeds a local circulation in the relay ramp of the SVFS (Figure 7). Deep-seated fluids are driven up to shallower depths through the dense multiscale fracturing of the relay ramp, which is produced by the accumulation of stress and maintained over time by the activity of the regional faults. This upwelling leads to a thermal anomaly (Figure 5) where the simulated values are 9 to 57 °C warmer than the surrounding undeformed foredeep.

The simulated fluid flow is a few orders of magnitude higher in the Schio-Vicenza fault zone and relay ramp than in the protolith, enforcing numerically the occurrence of preferential flow paths in the system. In particular, the highest temperatures and fluxes are modeled along the DE reproducing the ESE-WNW trending extensional open fractures deforming the EuGF bedrock. This result, which is corroborated by the experimental variogram map of the thermal aquifer transmissivity and outcrop data (Fabbri, 1997; Pola, Gandin, et al., 2014), physically validates the importance of fluid flow through open fractures as a predominant process in the EuGF. These fractures represent a preferential flow path in the subsurface and drive thermal waters up to the surface, clustering them to form thermal springs.

Spatial correspondence between increased temperatures and fluid flows suggests that the Euganean thermal anomaly results from high local convection in the relay ramp induced by fracturing and enforced by slight anomalous heat flow. The onset of the simulated anomaly cannot be produced by a purely conductive process or by a local increase in radiogenic heat associated with volcanic bodies. The former process develops a temperature distribution similar to that obtained from the steady-state simulation, which does not conform the field measurements, while the latter produces a slight increase (Figure 8a). Nevertheless, volcanic rocks influence the isotopic content of the thermal water as suggested by Ra, Rn, and He isotopes analyses (Gherardi et al., 2000; Mayer et al., 2015). These results confirm that structural causative processes at regional and local scales are crucial to the development of the thermal system, supporting the conceptual model of the EuGS. Furthermore, important feedback to the conceptual model itself is obtained. Temperatures of 100 °C at the maximum explored depth in the EuGF (1 km deep) and of 140 °C below the principal reservoir are simulated in the hottest section of the thermal anomaly. These results are interesting both for the conceptual modeling and the utilization scenarios of the resource. Although isotopic fractionation between CO_2 and CH_4 pointed to temperatures of 170 to 245 °C (Gherardi et al., 2000), this geothermometer was not included in previous conceptual modeling due to its scarce data set, and the maximum temperature in the system was considered to reach 100 °C (Pola, Fabbri, Piccinini, & Zampieri, 2015). The possible occurrence of water of temperatures higher than that currently exploited could lead to new uses of the Euganean thermal resource (e.g., energy production and district heating), integrating current balneotherapeutic uses during low tourism seasons.

In addition to these local implications, the performed modeling offers useful feedback from a regional point of view. Although approximately 60% of the modeled outflow is fed by the fault zone, the protolith provides approximately 30%. These ratios should be carefully considered from a quantitative point of view since they could be affected by the modeling approach and by the parametrization. Qualitatively, this result evidences an impact of the fluid flow through the protolith on the local flow in the relay ramp. This could result in different water/rock interactions in the system and variable residence time of waters, explaining the observed variability of the ^{14}C measurements (Boaretto et al., 2003). Furthermore, the modeling indirectly provides feedback to the regional structural setting. Fault geometries in northern and southern parts of the SVFS were obtained from seismic and structural data (Pola, Ricciato, et al., 2014), while the central part close to the Euganean Hills was established from regional gravimetric maps and indirect structural analyses (Pola, Fabbri, Piccinini, & Zampieri, 2015; Pola, Gandin, et al., 2014). A breaching fault could kinematically link the regional faults, but such a structure would develop a thermal anomaly (Figure 8b) that does not reproduce the field data. This result corroborates the need for a wide fractured area to produce the EuGF, which is compatible with the "relay ramp interpretation".

Based on the results of this work, the EuGS can be cataloged as a convective-dominated nonmagmatic geothermal play in which fracturing is the main factor enhancing convection. The importance of active faults was highlighted in Moeck (2014), but the reported case studies were limited to regional extensional settings in which high heat flows favored by crustal thinning combined with fracturing to enforce the convective process. Although some analogies can be found, the present case study of the EuGS proves that favorable conditions for increased convection can be found in other tectonic regimes. The system is located in the foreland basin of three surrounding chains (i.e., Apennines, Dinarides, and Eastern Southern Alps) that has been deformed by a multiphase compressional regime since the Late Eocene (Fantoni et al., 2002). Regional strike-slip segments of the SVFS linked through an interaction zone and the current regional stress axes oriented obliquely to its boundaries develop a local extension forming a pattern of both tensile and shear fractures, as observed in transtensional stepovers (De Paola et al., 2007). This geological setting increases fracturing and local permeability field of the bedrock,

favoring an enhanced convective process in a region where the heat flow is slightly higher than the average value of continental crust (70–80 mW/m^2 versus 60 mW/m^2; Pasquale et al., 2014a, 2014b). This fracturing-induced convection can lead to temperatures higher than exploited or expect values without the presence of an intense heat source.

The results of this study may lead to new uses of several worldwide low-temperature geothermal fields for which surficial manifestations could be affected by mixing with cold waters and deep original resources could be partially sealed or unexplored. Multidisciplinary investigations on the geochemical features of the thermal water and on the regional and local geological and hydrogeological settings are crucial to establish the main features of this kind of resources. Their results integrated into a robust conceptual model can be physically validated by numerical modeling. Simulations can direct further explorations and can be used to support or reject some hypotheses that may be difficult to test with other methods.

The numerical modeling approach is a crucial factor: the explicit discrete fracture approach (Bundschuh & Suárez Arriaga, 2010) permits one to reproduce faults and fractures over a wide range of length scales (cm to km scales), accounting for their impact on local convection. This approach is particularly suited for simulations of thermal systems controlled by major faults and the associated fractured reservoirs. The correct implementation of the fault and fracture systems driving the thermal fluid flow, and in general of the geological setting, within the model is crucial to determine their impact on the thermal system development. However, a comprehensive assessment of regional and local geological and physical processes within a unique model is far beyond the present computing capabilities (Scheck-Wenderoth et al., 2014). A balance between geological and numerical aspects can be achieved simplifying the geological, hydrogeological, and thermal settings, thus diminishing the computational effort for solving the fluid flow and heat transport equations. This problem was partially overcome in this study employing (i) a kinematically plausible reconstruction of the local fracture network based on structural data and (ii) a hydrogeological parametrization based on local measurements.

The workflow and the modeling approach employed in this work can be profitably used for (i) assessing the physical processes driving a thermal system at regional scale, (ii) initial regional simulations that are the basis for a local modeling, and (iii) modeling thermal systems with a limited amount of available data. The latter occurs in many, regional and intermediate scale, low-temperature, geothermal systems characterized by a few emergences of thermal waters and a limited data set of hydrogeological and temperature measurements (e.g., Borović et al., 2019). Although these geothermal resources are widespread, they are poorly investigated and they are generally endangered by inadequate extraction plans. The correct assessment of their geothermal potential favored and supported by an adequate numerical modeling could open new utilization scenarios for several low-temperature geothermal resource that could represent a paramount resource for local communities.

5. Conclusions

This work elucidates geological and physical processes developing a low-temperature thermal resource in NE Italy through conceptual and numerical modeling. Both approaches point to the primary role of existing regional and local faults and fractures in regional and local fluid flows. Highly permeable regional fault zones enhance the fluid flow in the carbonate reservoir, while dense fracturing associated with a relay ramp favors a local increase of convection, the rapid upwelling of hot fluids, and the development of an economically profitable geothermal resource. The occurrence of preferential flow path in the system is numerically quantified for the first time by the performed simulations. Despite its physical validation, the numerical modeling offers important feedback on the conceptual model. Temperatures in the unexplored parts of the thermal field and below the principal reservoir are higher than the expected values reaching 100 and 140 °C, respectively. In addition, the modeling results prove that the radiogenic volcanic bodies, which locally intrudes the reservoir, mostly influence the isotopic content of thermal water rather than its temperature.

This case study and the performed modeling can serve as an analog for low-temperature geothermal resources hosted in carbonate formations and controlled by faults. The numerical modeling applied as a supportive and integrative tool for conceptual modeling is effective in the investigation of low-temperature geothermal resources. Such resources have not been widely studied, but they should be considered as

potential targets for detailed geothermal exploration. The fracturing of bedrock associated with favorable geological setting could produce a local increment of the convection that usually occurs in active volcanic areas or in extensional basins with high heat flows. Such enhanced convection could lead to higher than expected temperatures in the unexplored sections of the resource, reaching values profitable for energy production or industrial processes. Therefore, low-temperature geothermal resources could represent a potential renewable heat and energy source for small-scale users or local communities since they are more common and widespread than high-temperature systems.

Acknowledgments
The model setup (i.e., geometry, distribution of parameters, and boundary and initial conditions) and results are available in the Mendeley Data database (https://doi.org/10.17632/zgpzr57b5b.1). This research was funded by the district authority of Euganean Geothermal Field (B.I.O.C.E.) within the project "Hydrogeological model of Euganean Geothermal System (EuGS)", grant to P. Fabbri. The authors would like to thank the B.I.O.C.E. for the technical support and fruitful discussions. We are grateful to the Associated Editor and the two anonymous reviewers for the helpful comments and critic revisions. The authors declare that they have no conflict of interest.

References

Antonelli, R., Barbieri, G., Dal Piaz, G. V., Dal Prà, A., De Zanche, V., Grandesso, P., et al. (1990). Carta geologica del Veneto 1: 250.000. Una storia di Cinquecento Milioni di Anni.

Antonelli, R., Callegari, E., Fabbri, P., & Sedea, R. (1993). Recenti contributi alla conoscenza dell'idrostruttura del bacino termale Euganeo (Padova). *GEAM - Geoengineering Environment and Mining*, *79*, 49–55.

Antonelli, R., Fabbri, P., Iliceto, V., Majorana, C., Previatello, P., Schrefler, B., & Sedea, R. (1995). The Geothermal Euganean Field. A subsidence modelling approach. *Proceedings of the World Geothermal Congress*, 1263–1268.

Aurighi, M., Cisotto, A., Dal Prà, A., Janza, M., Mariani, R., Nordio, M., et al. (2004). *Il carsismo nel Veneto-Carta idrogeologica dell'Altopiano dei Sette Comuni*. Venezia: Regione Veneto.

Baietto, A., Cadoppi, P., Martinotti, G., Perello, P., Perrochet, P., & Vuataz, F. D. (2008). Assessment of thermal circulations in strike-slip fault systems: The Terme di Valdieri case (Italian western Alps). *Geological Society, London, Special Publications*, *299*(1), 317–339. https://doi.org/10.1144/SP299.19

Baiocchi, A., Lotti, F., & Piscopo, V. (2013). Impact of groundwater withdrawals on the interaction of multi-layered aquifers in the Viterbo geothermal area (central Italy). *Hydrogeology Journal*, *21*(6), 1339–1353. https://doi.org/10.1007/s10040-013-1000-5

Bartoli, O., Meli, S., Bergomi, M. A., Sassi, R., Magaraci, D., & Liu, D.-Y. (2015). Geochemistry and zircon U-Pb geochronology of magmatic enclaves in trachytes from the Euganean Hills (NE Italy): Further constraints on Oligocene magmatism in the eastern Southern Alps. *European Journal of Mineralogy*, *27*(2), 161–174. https://doi.org/10.1127/ejm/2015/0027-2425

Bassani, M., Bressan, M., Ghedini, F., Favaretto, I., Ghedini, F., Busana, M. S., et al. (2012). *Aquae Patavinae: Montegrotto Terme e il termalismo in Italia; aggiornamenti e nuove prospettive di valorizzazione; atti del II convegno nazionale, Padova, 14-15 giugno 2011*. Padova: Padova University Press.

Bense, V. F., Gleeson, T., Loveless, S. E., Bour, O., & Scibek, J. (2013). Fault zone hydrogeology. *Earth-Science Reviews*, *127*, 171–192. https://doi.org/10.1016/j.earscirev.2013.09.008

Blasco, M., Auqué, L. F., Gimeno, M. J., Acero, P., & Asta, M. P. (2017). Geochemistry, geothermometry and influence of the concentration of mobile elements in the chemical characteristics of carbonate-evaporitic thermal systems. The case of the Tiermas geothermal system (Spain). *Chemical Geology*, *466*(July), 696–709. https://doi.org/10.1016/j.chemgeo.2017.07.013

Boaretto, E., Carmi, I., Fabbri, P., Heinemeier, J., Sartori, S., Sveinbjornsdottir, A.E., & Yechieli, Y. (2003). Radiocarbon in thermal and fresh groundwater in Veneto Region, Northern Italy. Paper presented at XVIII International Radiocarbon Conference, Wellington, New Zeland

Borović, S., Pola, M., Bačani, A., & Urumović, K. (2019). Constraining the recharge area of a hydrothermal system in fractured carbonates by numerical modelling. *Geothermics*, *82*, 128–149. https://doi.org/10.1016/j.geothermics.2019.05.017

Bourdon, B., Turner, S., Henderson, G. M., & Lundstrom, C. C. (2003). Uranium-series geochemistry. *Reviews in Mineralogy and Geochemistry*, *52*(1), 1–21. https://doi.org/10.2113/0520001

Brehme, M., Blöcher, G., Cacace, M., Kamah, Y., Sauter, M., & Zimmermann, G. (2016). Permeability distribution in the Lahendong geothermal field: A blind fault captured by thermal–hydraulic simulation. *Environmental Earth Sciences*, *75*(14), 1–11. https://doi.org/10.1007/s12665-016-5878-9

Brogi, A., Capezzuoli, E., Aqué, R., Branca, M., & Voltaggio, M. (2010). Studying travertines for neotectonics investigations: Middle–Late Pleistocene syn-tectonic travertine deposition at Serre di Rapolano (Northern Apennines, Italy). *International Journal of Earth Sciences*, *99*(6), 1383–1398. https://doi.org/10.1007/s00531-009-0456-y

Brogi, A., Capezzuoli, E., Buracchi, E., & Branca, M. (2012). Tectonic control on travertine and calcareous tufa deposition in a low-temperature geothermal system (Sarteano, Central Italy). *Journal of the Geological Society*, *169*(4), 461–476. https://doi.org/10.1144/0016-76492011-137

Bundschuh, J., & Suárez Arriaga, M. C. (2010). *Introduction to the numerical modeling of groundwater and geothermal systems: Fundamentals of mass, energy and solute transport transport in poroelastic rocks*. London: CRC Press.

Cacace, M., & Jacquey, A. B. (2017). Flexible parallel implicit modelling of coupled thermal–hydraulic–mechanical processes in fractured rocks. *Solid Earth*, *8*(5), 921–941. https://doi.org/10.5194/se-8-921-2017

Cherubini, Y., Cacace, M., Scheck-Wenderoth, M., Moeck, I., & Lewerenz, B. (2013). Controls on the deep thermal field: Implications from 3-D numerical simulations for the geothermal research site Groß Schönebeck. *Environmental Earth Sciences*, *70*(8), 3619–3642. https://doi.org/10.1007/s12665-013-2519-4

Chiodini, G., Frondini, F., & Marini, L. (1995). Theoretical geothermometers andPCO2 indicators for aqueous solutions coming from hydrothermal systems of medium-low temperature hosted in carbonate-evaporite rocks. Application to the thermal springs of the Etruscan Swell, Italy. *Applied Geochemistry*, *10*(3), 337–346. https://doi.org/10.1016/0883-2927(95)00006-6

Consorzio Terme Euganee. (2016). Thermae Abano Montegrotto-Momenti da vivere. Retrieved from: http://www.consorziotermeeuganee.it/wp-content/uploads/2015/07/CARTELLA-STAMPA_low_ita-ok.pdf.

Cucato, M., De Vecchi, G. P., Mozzi, P., Abbà, T., Paiero, R., & Sedea, R.(2012) Note illustrative della Carta geologica d'Italia alla scala 1: 50.000, foglio 147-Padova Sud. ISPRA-Servizio Geologico d'Italia–Regione Veneto, LTS Land Technology & Services, Padova & Treviso.

Cuoco, E., Minissale, A., Leo, D., Magda, A., Tamburrino, S., Iorio, M., & Tedesco, D. (2017). Fluid geochemistry of the Mondragone hydrothermal systems (southern Italy): Water and gas compositions vs. geostructural setting. *International Journal of Earth Sciences*, *106*(7), 2429–2444. https://doi.org/10.1007/s00531-016-1439-4

Curewitz, D., & Karson, J. A. (1997). Structural settings of hydrothermal outflow: Fracture permeability maintained by fault propagation and interaction. *Journal of Volcanology and Geothermal Research*, *79*(3–4), 149–168. https://doi.org/10.1016/S0377-0273(97)00027-9

De Paola, N., Holdsworth, R. E., Collettini, C., Mccaffrey, K. J. W., & Barchi, M. R. (2007). The structural evolution of dilational stepovers in regional transtensional zones. *Geological Society, London, Special Publications*, *290*(1), 433–445. https://doi.org/10.1144/SP190.17

Della Vedova, B., Vecellio, C., Bellani, S., & Tinivella, U. (2008). Thermal modelling of the Larderello geothermal field (Tuscany, Italy). *International Journal of Earth Sciences*, *97*(2), 317–332. https://doi.org/10.1007/s00531-007-0249-0

Dickson, M. H., & Fanelli, M. (2013). Geothermal energy: Utilization and technology. Routledge.

Diersch, H.-J. G. (2014). *FEFLOW*. Berlin, Heidelberg: Springer Berlin Heidelberg. https://doi.org/10.1007/978-3-642-38739-5

Domenico, P. A., & Schwartz, F. W. (1998). *Physical and chemical hydrogeology*, (Vol. 506). New York: Wiley.

Fabbri, P. (1997). Transmissivity in the geothermal Euganean basin: A geostatistical analysis. *Ground Water*, *35*(5), 881–887. https://doi.org/10.1111/j.1745-6584.1997.tb00156.x

Fabbri, P. (2001). Probabilistic assessment of temperature in the Euganean geothermal area (Veneto region, NE Italy). *Mathematical Geology*, *33*(6), 745–760. https://doi.org/10.1023/A:1011030900322

Fabbri, P., Pola, M., Piccinini, L., Zampieri, D., Roghel, A., & Dalla Libera, N. (2017). Monitoring, utilization and sustainable development of a low-temperature geothermal resource: A case study of the Euganean Geothermal Field (NE, Italy). *Geothermics*, *70*, 281–294. https://doi.org/10.1016/j.geothermics.2017.07.002

Fabbri, P., & Trevisani, S. (2005). Spatial distribution of temperature in the low-temperature geothermal Euganean field (NE Italy): A simulated annealing approach. *Geothermics*, *34*(5), 617–631. https://doi.org/10.1016/j.geothermics.2005.07.001

Faccenda, M., Bressan, G., & Burlini, L. (2007). Seismic properties of the upper crust in the central Friuli area (northeastern Italy) based on petrophysical data. *Tectonophysics*, *445*(3–4), 210–226. https://doi.org/10.1016/j.tecto.2007.08.004

Fantoni, R., Catellani, D., Merlini, S., Rogledi, S., & Venturini, S. (2002). La registrazione degli eventi deformativi cenozoici nell'avampaese Veneto-Friulano. *Memorie Della Società Geologica Italiana*, *57*, 301–313.

Fantoni, R., & Franciosi, R. (2010). Tectono-sedimentary setting of the Po Plain and Adriatic foreland. *Rendiconti Lincei*, *21*(S1), 197–209. https://doi.org/10.1007/s12210-010-0102-4

Faulds, J. E., Hinz, N. H., Dering, G. M., & Siler, D. L. (2013). The hybrid model—The most accommodating structural setting for geothermal power generation in the Great Basin, Western USA. *Geothermal Resources Council Transactions*, *37*, 4–10.

Faulkner, D. R., Jackson, C. A. L., Lunn, R. J., Schlische, R. W., Shipton, Z. K., Wibberley, C. A. J., & Withjack, M. O. (2010). A review of recent developments concerning the structure, mechanics and fluid flow properties of fault zones. *Journal of Structural Geology*, *32*(11), 1557–1575. https://doi.org/10.1016/j.jsg.2010.06.009

Fossen, H., & Rotevatn, A. (2016). Fault linkage and relay structures in extensional settings—A review. *Earth-Science Reviews*, *154*, 14–28. https://doi.org/10.1016/j.earscirev.2015.11.014

Frondini, F. (2008). Geochemistry of regional aquifer systems hosted by carbonate-evaporite formations in Umbria and southern Tuscany (central Italy). *Applied Geochemistry*, *23*(8), 2091–2104. https://doi.org/10.1016/j.apgeochem.2008.05.001

Fusari, A., Carroll, M. R., Ferraro, S., Giovannetti, R., Giudetti, G., Invernizzi, C., et al. (2017). Circulation path of thermal waters within the Laga foredeep basin inferred from chemical and isotopic (δ18O, δD, 3H, 87Sr/86Sr) data. *Applied Geochemistry*, *78*, 23–34. https://doi.org/10.1016/j.apgeochem.2016.11.021

Germinario, L., Siegesmund, S., Maritan, L., & Mazzoli, C. (2017). Petrophysical and mechanical properties of Euganean trachyte and implications for dimension stone decay and durability performance. *Environmental Earth Sciences*, *76*(21), 1–21. https://doi.org/10.1007/s12665-017-7034-6

Gherardi, F., Panichi, C., Caliro, S., Magro, G., & Pennisi, M. (2000). Water and gas geochemistry of the Euganean and Berician thermal district (Italy). *Applied Geochemistry*, *15*(4), 455–474. https://doi.org/10.1016/S0883-2927(99)00056-6

Goldscheider, N., Mádl-Szőnyi, J., Erőss, A., & Schill, E. (2010). Review: Thermal water resources in carbonate rock aquifers. *Hydrogeology Journal*, *18*(6), 1303–1318. https://doi.org/10.1007/s10040-010-0611-3

Gunn, J., Bottrell, S. H., Lowe, D. J., & Worthington, S. R. H. (2006). Deep groundwater flow and geochemical processes in limestone aquifers: Evidence from thermal waters in Derbyshire, England, UK. *Hydrogeology Journal*, *14*(6), 868–881. https://doi.org/10.1007/s10040-006-0022-7

Ingebritsen, S. E., Geiger, S., Hurwitz, S., & Driesner, T. (2010). Numerical simulation of magmatic hydrothermal systems. *Reviews of Geophysics*, *48*, RG1002. https://doi.org/10.1029/2009RG000287

Lund, J. W., & Boyd, T. L. (2016). Direct utilization of geothermal energy 2015 worldwide review. *Geothermics*, *60*, 66–93. https://doi.org/10.1016/j.geothermics.2015.11.004

Magri, F., Akar, T., Gemici, U., & Pekdeger, A. (2012). Numerical investigations of fault-induced seawater circulation in the Seferihisar-Balçova Geothermal system, western Turkey. *Hydrogeology Journal*, *20*(1), 103–118. https://doi.org/10.1007/s10040-011-0797-z

Mandruzzato, S. (1789). *Trattato dei Bagni di Abano*. Padova: Penada Giovambattista e figli.

Massironi, M., Zampieri, D., & Caporali, A. (2006). Miocene to present major fault linkages through the Adriatic indenter and the Austroalpine-Penninic collisional wedge (Alps of NE Italy). *Geological Society, London, Special Publications*, *262*(1), 245–258. https://doi.org/10.1144/GSL.SP.2006.262.01.15

Mayer, A., Pola, M., Fabbri, P., Piccinini, L., & Zampieri, D. (2015). Radium-radon-actinium systematic in geothermal groundwater: Constraints for groundwater upwelling-time in the Euganean geothermal field (Italy). Paper presented at International Symposium on Isotope hydrology "Revisiting Foundations and Exploring Frontiers", Wien, Austria.

Moeck, I. S. (2014). Catalog of geothermal play types based on geologic controls. *Renewable and Sustainable Energy Reviews*, *37*, 867–882. https://doi.org/10.1016/j.rser.2014.05.032

Montanari, D., Minissale, A., Doveri, M., Gola, G., Trumpy, E., Santilano, A., & Manzella, A. (2017). Geothermal resources within carbonate reservoirs in western Sicily (Italy): A review. *Earth-Science Reviews*, *169*(December 2016), 180–201. https://doi.org/10.1016/j.earscirev.2017.04.016

Norinelli, A. (1979). Anomalie aeromagnetiche del distretto eruttivo Euganeo-Berico. *Memorie Di Scienze Geologiche*, *32*, 4–8.

Norton, D., & Panichi, C. (1978). Determination of the sources and circulation paths of thermal fluids: The Abano region, northern Italy. *Geochimica et Cosmochimica Acta*, *42*(8), 1283–1294. https://doi.org/10.1016/0016-7037(78)90122-9

Pang, J., Pang, Z., Lv, M., Tian, J., & Kong, Y. (2018). Geochemical and isotopic characteristics of fluids in the Niutuozhen geothermal field, North China. *Environmental Earth Sciences*, *77*(1), 1–21. https://doi.org/10.1007/s12665-017-7171-y

Pasquale, V., Chiozzi, P., & Verdoya, M. (2013). Evidence for thermal convection in the deep carbonate aquifer of the eastern sector of the Po Plain, Italy. *Tectonophysics*, *594*, 1–12. https://doi.org/10.1016/j.tecto.2013.03.011

Pasquale, V., Gola, G., Chiozzi, P., & Verdoya, M. (2011). Thermophysical properties of the Po Basin rocks. *Geophysical Journal International*, *186*(1), 69–81. https://doi.org/10.1111/j.1365-246X.2011.05040.x

Pasquale, V., Verdoya, M., & Chiozzi, P. (2014a). *Geothermics*. Cham: Springer International Publishing. https://doi.org/10.1007/978-3-319-02511-7

Pasquale, V., Verdoya, M., & Chiozzi, P. (2014b). Heat flow and geothermal resources in northern Italy. *Renewable and Sustainable Energy Reviews*, *36*, 277–285. https://doi.org/10.1016/j.rser.2014.04.075

Pepin, J., Person, M., Phillips, F., Kelley, S., Timmons, S., Owens, L., et al. (2015). Deep fluid circulation within crystalline basement rocks and the role of hydrologic windows in the formation of the Truth or Consequences, New Mexico low-temperature geothermal system. *Geofluids*, *15*(1–2), 139–160. https://doi.org/10.1111/gfl.12111

Perello, P., Marini, L., Martinotti, G., & Hunziker, J. C. (2001). The thermal circuits of the Argentera Masssif (western Alps, Italy). An example of low-enthalpy geothermal resources controlled by Neogene alpine tectonics. Ecologae Geol.Helv. https://doi.org/10.5169/seals-168878

Pola, M., Fabbri, P., Gandin, A., Soligo, M., Tuccimei, P., Deiana, R., & Zampieri, D. (2011). The montirone travertine mound: A multidisciplinary approach: Implications for the euganean geothermal field. *Rendiconti Online della Società Geologica Italiana*, *16*, 28–29.

Pola, M., Fabbri, P., Piccinini, L., Dalla Libera, N., Zampieri, D., Roghel, A., et al. (2016). Mapping the variation of the potentiometric level of the Euganean thermal aquifer and relationship with the exploitation. *Rendiconti Online della Società Geologica Italiana*, *41*, 284–287. https://doi.org/10.3301/ROL.2016.149

Pola, M., Fabbri, P., Piccinini, L., Marcolongo, E., Rosignoli, A., Zampieri, D., et al. (2015). Anthropic impact on thermal aquifer: The case study of the Euganean Geothermal Field (NE Italy). *Rendiconti Online della Società Geologica Italiana*, *35*, 240–243. https://doi.org/10.3301/ROL.2015.110

Pola, M., Fabbri, P., Piccinini, L., & Zampieri, D. (2015). Conceptual and numerical models of a tectonically-controlled geothermal system: A case study of the Euganean Geothermal System, Northern Italy. *Central European Geology*, *58*(1–2), 129–151. https://doi.org/10.1556/24.58.2015.1-2.9

Pola, M., Gandin, A., Tuccimei, P., Soligo, M., Deiana, R., Fabbri, P., & Zampieri, D. (2014). A multidisciplinary approach to understanding carbonate deposition under tectonically controlled hydrothermal circulation: A case study from a recent travertine mound in the Euganean hydrothermal system, northern Italy. *Sedimentology*, *61*(1), 172–199. https://doi.org/10.1111/sed.12069

Pola, M., Ricciato, A., Fantoni, R., Fabbri, P., & Zampieri, D. (2014). Architecture of the western margin of the North Adriatic foreland:The Schio-Vicenza fault system. *Italian Journal of Geosciences*, *133*(2), 223–234. https://doi.org/10.3301/IJG.2014.04

Rotevatn, A., & Peacock, D. C. P. (2018). Strike-slip reactivation of segmented normal faults: Implications for basin structure and fluid flow. *Basin Research*, *30*(6), 1264–1279. https://doi.org/10.1111/bre.12303

Rowland, J. V., & Sibson, R. H. (2004). Structural controls on hydrothermal flow in a segmented rift system, Taupo Volcanic Zone, New Zealand. *Geofluids*, *4*(4), 259–283. https://doi.org/10.1111/j.1468-8123.2004.00091.x

Savage, H. M., & Brodsky, E. E. (2011). Collateral damage: Evolution with displacement of fracture distribution and secondary fault strands in fault damage zones. *Journal of Geophysical Research*, *116*, B03405. https://doi.org/10.1029/2010JB007665

Scheck-Wenderoth, M., Cacace, M., Maystrenko, Y. P., Cherubini, Y., Noack, V., Kaiser, B. O., et al. (2014). Models of heat transport in the Central European Basin System: Effective mechanisms at different scales. *Marine and Petroleum Geology*, *55*, 315–331. https://doi.org/10.1016/j.marpetgeo.2014.03.009

Scott, B. J., Mroczek, E. K., Burnell, J. G., Zarrouk, S. J., Seward, A., Robson, B., & Graham, D. J. (2016). The Rotorua Geothermal Field: An experiment in environmental management. *Geothermics*, *59*, 294–310. https://doi.org/10.1016/j.geothermics.2015.09.004

Strati, V., Baldoncini, M., Bezzon, G. P., Broggini, C., Buso, G. P., Caciolli, A., et al. (2015). Total natural radioactivity, Veneto (Italy). *Journal of Maps*, *11*(4), 545–551. https://doi.org/10.1080/17445647.2014.923348

Tositti, L., Cinelli, G., Brattich, E., Galgaro, A., Mostacci, D., Mazzoli, C., et al. (2017). Assessment of lithogenic radioactivity in the Euganean Hills magmatic district (NE Italy). *Journal of Environmental Radioactivity*, *166*(Pt 2), 259–269. https://doi.org/10.1016/j.jenvrad.2016.07.011

Viganò, A., Bressan, G., Ranalli, G., & Martin, S. (2008). Focal mechanism inversion in the Giudicarie–Lessini seismotectonic region (Southern Alps, Italy): Insights on tectonic stress and strain. *Tectonophysics*, *460*(1–4), 106–115. https://doi.org/10.1016/j.tecto.2008.07.008

Volpi, G., Magri, F., Frattini, P., Crosta, G. B., & Riva, F. (2017). Groundwater-driven temperature changes at thermal springs in response to recent glaciation: Bormio hydrothermal system, Central Italian Alps. *Hydrogeology Journal*, *25*(7), 1967–1984. https://doi.org/10.1007/s10040-017-1600-6

Vosteen, H.-D., Rath, V., Clauser, C., & Lammerer, B. (2003). The thermal regime of the Eastern Alps from inversion analyses along the TRANSALP profile. *Physics and Chemistry of the Earth, Parts A/B/C*, *28*(9–11), 393–405. https://doi.org/10.1016/S1474-7065(03)00060-3

Vosteen, H.-D., & Schellschmidt, R. (2003). Influence of temperature on thermal conductivity, thermal capacity and thermal diffusivity for different types of rock. *Physics and Chemistry of the Earth, Parts A/B/C*, *28*(9–11), 499–509. https://doi.org/10.1016/S1474-7065(03)00069-X

Yang, P., Cheng, Q., Xie, S., Wang, J., Chang, L., Yu, Q., et al. (2017). Hydrogeochemistry and geothermometry of deep thermal water in the carbonate formation in the main urban area of Chongqing, China. *Journal of Hydrology*, *549*(April 2011), 50–61. https://doi.org/10.1016/j.jhydrol.2017.03.054

Zampieri, D. (1995). Tertiary extension in the southern Trento Platform, Southern Alps, Italy. *Tectonics*, *14*(3), 645–657. https://doi.org/10.1029/94TC03093